

# Reply to S. Cornford's Review on "Thermal structure and basal sliding parametrisation at Pine Island Glacier - a 3D full-Stokes model study"

First we would like to thank the reviewer for his constructive and helpful comments. Below you find a point-by-point response to them.

## 1 General comments

**Reviewer1:** The paper investigates basal traction laws based on measured bed roughness for PIG, studying them using a rather sophisticated new Stokes model. A typical PIG flow experiment finds the basal traction  $\tau_b$  through an inverse problem and then assumes a physical law of the form  $C \tau_b = u^{m-1} \mathbf{u}$  for use in prognostic simulations, holding  $C(x, y)$  constant in time. The authors compare this conventional kind of approach with two roughness based laws, with the roughness derived from measurements (measured along flight lines and extended to the whole region). The resulting  $C$  would still be constant in time (unless some roughness evolution model was added), but its time independence would have some more physical justification.

If the model had reproduced all the features of the flow using these measurements, this would support the conventional approach, but perhaps supplant it. However, the model does not reproduce the observations as well as it does with an inferred  $C$  (even when the inversion, as in this paper, is not as sophisticated as elsewhere) and so the authors find that  $C$  is not just a function of roughness but other fields that are not observed – which could include roughness at the scales below those measured, or other physics, including physics that could evolve on short – such as basal hydrology. Nonetheless, the paper shows that many of the flow features can be accounted for by measured roughness, so that the proposed laws could form part of more complex laws, and I suggest could be directly useful in, for example, paleo ice stream simulations where the ice has gone but bed roughness data might be available.

The friction laws themselves are presented are in the results section, but I think they are more important to this paper than the description of the Stokes model, so should be described earlier. I also think that the sections describing the laws need some revision, in particular the manuscript needs to summarize the way in which the one-parameter roughness was measured (inferred from airborne radar, in Rippin 2011, estimated to be sensitive to roughness wavelengths  $> 500$  m), and explain the calculation of the two-parameter roughness in more detail.

**Answer:** We agree that the roughness data and the sliding laws need more attention and also need to be described earlier in the manuscript. We therefore added another Section titled **Methods: roughness data and sliding laws**, which is included right after the model description. There in detail the derivation of the roughness data is explained. It is also emphasised that the single-parameter roughness was already presented in Rippin et al. 2011, while the two-parameter

roughness measure was especially calculated for this study. The sliding laws are also described in more detail and a better overview about the connections of the different formulations and parameters is given.

**R1:** At the same time, a temperature distribution is estimated. This is a useful result on its own.

## 2 Specific comments

**R1:** L10: Some inverse problems seek effective viscosity (or some equivalent) as well as or instead of a basal friction coefficient in some inverse problems. Especially in the ice shelf, but to some extent in shear margins, effective viscosity determines the flow. This is mentioned in the discussion.

**Answer:** We focussed in this study on the parameterization of basal sliding and therefore did not mention in detail the inversion for effective viscosity. One advantage of our model is, that we managed to solve for the temperature also in the ice shelf. Therefore the need to invert for effective viscosity there is not as crucial. Nonetheless we do recognise the effective viscosity as being especially important in the shear margins, and address some of the deviations in surface velocity to this shortcoming.

**Changes:** Changed P4914, L8-10 to: Inversion methods are commonly applied to reproduce the complex surface flow structure at Pine Island Glacier, which use information of the observed surface velocity field, to constrain, *among other things*, basal sliding.

Changed P4915, L16-18 to: These methods use the measured surface velocity field to invert for basal properties *or effective viscosity* and to adjust basal sliding parameters.

**R1:** P4916 : 'Changes in basal conditions, by for example grounding line migration (Park et al., 2013), subglacial erosion (Smith et al., 2012; Rippin et al., 2014) or dynamic hydraulic systems, can not be considered with this approach.'

I agree that subglacial erosion or evolving hydrology defeat a inverted C that is constant in time, but I don't think that is true for grounding line retreat – the evolution of C (becoming zero in newly grounded regions) is straightforward in that case.

**Answer:** We agree that grounding line retreat could be considered nonetheless.

**Changes:** Changed P4916, L4-6 to: Changes in basal conditions, by for example subglacial erosion (Smith et al., 2012; Rippin et al., 2014) or dynamic hydraulic systems, can not be considered with this approach.

**R1:** 2.3.2.

Temperature transport includes strong advection, but you don't say whether this affects your numerical scheme (you just say that you use linear elements). Do

you ensure the local Peclet number is always low by choosing a mesh, or add artificial diffusion, or use DG methods, or something else?

**Answer:** We do use stabilization methods provided by COMSOL, which we forgot to mention. The details are described below.

**Changes:** We added a paragraph in Sect. 2.3.2: To avoid numerical instabilities due to strong temperature advection, and thus to ensure that the element Péclet number is always  $< 1$ , we use consistent stabilization methods provided by COMSOL Multiphysics®. Equation (7) is solved using a Galerkin Least Square (GLS) formulation (Codina, 1998) in streamline direction and crosswind diffusion (Hauke and Hughes, 1998) orthogonal to the streamline direction. The chosen stabilization methods add less numerical diffusion the closer the numerical solution comes to the exact solution (COMSOL, 2012).

**R1:** You say that all Dirichlet conditions are implemented as weak constraints. Does this mean you are adding a source term  $S$  to the equations on the basal face along the lines of  $S=a(T_0-T)$ , so that as  $a \rightarrow \infty$  the solution approaches  $T_0=T$ . If so, you are actually implementing a Robin condition (which is fine).

**Answer:** Weak constraints satisfy a condition in a weak sense, i.e. in integral sense over the entire boundary of the element. They are different to Robin conditions.

Pointwise constraints:  $u(x) = f(x)$  for  $x$  on  $\Gamma$  (boundary)

Weak constraints:  $\int_{\Gamma} u \varphi \delta x = \int_{\Gamma} f \varphi \delta x$  with  $\varphi$  being the test function.

**Changes:** Changed P4923, L10-11 (where „Weak constraints“ are first mentioned) to: The kinematic condition at the ice base is implemented as a weak constraint, for stability reasons. Weak constraints apply boundary conditions in an integral sense and are therefore not as strict. They stand in contrast to pointwise constraints, which force the nodal value to the constraint and can thus lead to numerical instability (COMSOL, 2012).

**R1:** Your heat flux condition looks like a softening of the step change around  $T_{b,max}$ , did you have problems with a sharp step?

**Answer:** Yes, it is a softening of the step change. A sharp step led to numerical instability and the model did not converge.

**Changes:** Added a sentence at the end of Sect. 2.3.2: The smoothing of the step function ensures numerical stability, which was not found with a sharp step.

**R1:** 2.3.3

I don't think that the aspect ratio requires an unstructured mesh (and indeed, several models use structured or block-structured meshes). Even the need for fine horizontal mesh resolution near the grounding line / shear margins is a little contentious, for example you might use high order elements instead. The figure looks as though you have extruded a 2D mesh of triangles vertically to get prisms with a vertical extent that varies only with thickness, (in which case you have

structure in the vertical direction). That could be because we can't see into the mesh - maybe you have finer vertical resolution in the regions with finer horizontal resolution. If so, is it possible to make a cut into the mesh figure to show that?

**Answer:** The original first sentence in Section 2.3.3 (*"The small aspect ratio of PIG (ratio of vertical to horizontal extent  $\epsilon = HL^{-1} \approx 10^{-3}$ ) requires an unstructured finite element mesh, to maximise the resolution while minimising the amount of elements."*) was not intended to say, that due to the small aspect ratio the unstructured mesh is mandatory, but it is very useful to maximise the resolution in regions of interest, while minimising the amount of elements. The higher mesh resolution around the grounding line is, as you say, not the only way to manage the steep gradients there, but it is a solution for this study that works well. Using high order elements – by the way – is not a very good solution in the case of sharp changes, since they expose Gibbs phenomena and would require additional filtering in order to control those.

It is true, that the mesh is structured in the vertical direction. We have 12 vertical layers everywhere, where the thickness varies only with ice thickness, which results in sigma layers.

**Changes:** We changed the paragraph to: To maximise the resolution while minimising the amount of elements, we use an unstructured finite element mesh, shown in Fig.2. The upper surface  $z_s$  is meshed first with triangles. The horizontal edge lengths are 5–500m at the grounding line and the calving front, 50–1000m at the inflow area and 100–2000m at the rest of the outer boundary. The resulting 2D surface mesh is extruded through the glacier geometry with a total of 12 vertical layers everywhere. The thickness of the vertical layers varies only with ice thickness. The spacing between the layers is refined towards the base. The ratio of the lowest to the upper most layer thickness is 0.01, leading to a thickness of the lowest layer of about 5m for a total ice thickness of 3000m. The final mesh consists of  $\sim 3.5 \times 10^5$  prism elements, which results in  $\sim 5 \times 10^6$  degrees of freedom (DOF), when solved for all variables.

#### **R1:** 2.3.4

Which direct linear solver: MUMPS? UMFPack ? A citation might be in order. I think this paragraph could do with some attention, although the meaning is clear to me, the grammar is a bit awkward. Especially, you say that you use a directed segregated solver which solves iteratively, which sounds self-refuting. I think that what you do is a kind of quasi-Newton iteration to solve a non-linear problem in  $u;p;T$  where you

1. Choose initial  $u^*;p^*;T^*$ ,
2. Use  $u^*;p^*;T^*$  to define a linear system which is solved directly to get  $u;p$
3. Use  $u;p;T^*$  to define a linear system which is solved directly for  $T$
4. Set  $u^*;p^*;T^* \leftarrow u;p;T$  and repeat 2-3 until your error estimate is small.

**Answer:** We used the direct solver Pardiso and added citations. And yes, what you write about the quasi-Newton iteration is correct. We rewrote Sect. 2.3.4 to make it clearer (see below).

**Changes:** We changed Sect. 2.3.4 to: For solving the nonlinear system, a direct segregated solver is used, which conducts a quasi-Newton iteration. It solves consecutively: first for the velocity  $u$  and the pressure  $p$ , and thereafter for the temperature  $T$  (Comsol, 2012). This allows for reduced working memory usage. For the remaining linear systems of equations the direct solver Pardiso (COMSOL (2012) and <http://www.pardiso-project.org/>, last access: 9 December 2014) is applied. While uncommon for such large numbers of DOF's, it proved to be computationally viable and robust, since all available iterative solvers exposed instabilities on this problem.

### **R1:** 3.3.2

Figure 5 could be replaced (or complemented) with a map of differences. With fig 5 as it is, you have to point out that the differences are exaggerated at low speeds and suppressed at high velocities, given the choice of log axes, which you need because so much of the glacier is slow. At the same time, there are maps to compare your results with in e.g Morlighem 2010. The same goes for figures 8 and 11.

**Answer:** A map of differences can be found in Wilkens, 2014 (Fig. 4.26). We choose to not show it here, as it would require elaborate description for the structure of the differences, which are partly related to the rheological treatment of shear margins and the inversion technique. We use the reference simulation to compare it to the roughness-related results. So the rheological treatment of the shear margins is consistent in all simulations.

Our focus of this study is not essentially to reproduce the surface flow field as precise as possible, but to understand basal sliding mechanisms and connect them to basal parameters.

Figure 5 shows in our opinion the difference between the simulated and measured velocities well. We will add some explanation in the figure caption for the logarithmic axes chosen. It is already mentioned in the main text (P4928, L23-24): *“The spread around the diagonal for lower velocities appears bigger, which is mainly due to the logarithmic axes chosen.”*

We decided to not compare our surface velocity field to the results from Morlighem et al., 2010, as our deviations to the measured field are much higher, would have to be explained in detail and is mainly due to the more sophisticated inversion technique they use. Here again it should be stated that the focus of this study was not to reproduce the field perfectly.

Comparing the results in Fig. 8 and 11 to the results of Morlighem et al., 2010 would give no further understanding of the findings. The differences in magnitude would be very large, which is why we compare the results in a qualitative manner.

**Changes:** We changed the caption of Figure 5 to: Observed surface velocity field  $|\mathbf{u}_{\text{obs}}|$  vs. reference surface velocity field  $|\mathbf{u}_{\text{s,ref}}|$ . The logarithmic scales exaggerate the spread around the low speeds. The angle offset  $\Delta\alpha$  between the vectors of the

surface velocity field  $\mathbf{u}_{\text{obs}}$  and the reference surface velocity field  $\mathbf{u}_{\text{s,ref}}$  is shown as the colour code.

### **R1: Technical corrections**

L8: Dependend → Depending

2.2.2 Stokes → Stress, or velocity

p4923, L18 :The temperature is *solved* for with linear elements : → discretized

p4925, L9 : ‘The basis data A. Le Brocq used are for the surface elevation from Bamber et al. (2009), which combines satellite radar and laser measurements. The ice thickness data is from Vaughan et al. (2006).’ could be something like ‘The Le Brocq data are based on the the surface elevation data of Bamber et al. (2009) and the ice thickness data of Vaughan et al. (2006)’.

**Answer:** Thanks for reading the manuscript carefully.

**Changes:** All technical corrections are included in the revised manuscript.

## Reply to Anonymous Review #2 on “Thermal structure and basal sliding parametrisation at Pine Island Glacier - a 3D full-Stokes model study”

First we would like to thank the reviewer for the constructive and helpful comments. Below you find a point-by-point response to them.

**Reviewer2:** In the paper the authors perform a surface-to-bed inversion for basal slipperiness using a numerical (full Stokes) flow model. They then compare the inverted (spatially variable) basal sliding parameter with two estimates of basal roughness.

**Answer:** This is not entirely correct. We do not simply compare the inverted sliding parameter with the basal roughness. This would mean we are comparing the fields  $\beta^2$  with for example the single-parameter roughness measure  $\xi$ . This would result in just comparing spatially varying fields. Instead we incorporate two different data sets of measured basal roughness into formulations for basal sliding. Since the model is thermo-mechanically coupled, the system evolves into a new equilibrium with sliding and non-sliding regions (at least for the first approach with the single-parameter roughness). Additionally the effect of basal water pressure is also included in the sliding law. Since the system consists of many unknowns, the outcome cannot be known afore.

**R2:** The main objective of the paper is, in the words of the authors: to connect measured basal properties to the parameterisation of basal sliding and therefore constrain basal sliding with physically justified assumptions.

Two estimates of basal roughness are used. One is a measure of basal roughness suggested by Li et al, 2010. If I understood correctly this measure is calculated directly by the authors.

**Answer:** This is correct, the two-parameter roughness measure was calculated by David Rippin especially for his study. It is based on the same data as the single-parameter roughness measure presented in Rippin et al. 2011.

**R2:** The other measure of roughness is based on Rippin et al, 2011. My understanding is that here previously published roughness estimates were used.

**Answer:** This is correct. We included now a paragraph which explicitly describes the roughness data, to make it less confusing. Additionally we changed the lines below.

**Changes:** Changed P4916, L20-24 to:

The first method matches a single-parameter basal roughness measure for PIG, as presented in Rippin et al. 2011, onto a basal sliding parameter. The second method is based on ideas from Li et al. 2010, where we use a two-parameter

basal roughness measure, especially calculated for this study, to connect basal roughness to basal sliding.

**R2:** If I've understood correctly, the roughness estimates are derived from the same bed-topography data set as the one used in the numerical model.

**Answer:** This is correct; they are both based on the data from Vaughan et al. 2006. Still the roughness measure and the bed-topography enter the model in different ways. The model geometry is built based on gridded data with 1 km spacing. The roughness measure is calculated based on along track sample spacing of the order of 30 m (cf. Rippin et al. 2011). Therefore higher resolution information is included in the roughness measure, even though it is also eventually gridded onto a 1 km grid. Since the roughness data and the use of it was not formulated in a comprehensible way previously, we included a whole new section describing the data and the sliding laws, included just after the model description and titled **Methods: roughness data and sliding laws**. In this section a paragraph states the differences (see below).

**Changes:** Included is a new section, including the paragraph:  
For PIG the single parameter roughness measure  $\xi$  was calculated by Rippin et al. 2011 from a RES data set generated in austral summer 2004/05 (Vaughan et al. 2006). It is the same data set the model geometry is based on (Sect. 2.3.5), still the roughness measure includes higher resolution information, as the derivation is based on along track sample spacing of the order of 30 m (cf. Rippin et al. 2011). Both data sets are then gridded with 1 km spacing.

**R2:** And this brings me to the main issue I have with the paper: If the bed of the numerical model is based on the same data set at these estimates of 'roughness', and since the numerical model calculates the effect of this bed on the flow, has the effect of the 'roughness' on the flow not already been modelled?

**Answer:** Although the model geometry and the roughness measure are based on the same data, they influence the flow behaviour on very different scales and with different mechanisms. A main key is here the different resolution, as mentioned by yourself. Maybe considering Weertman's original ideas can bring some clarification. He formulated a sliding law by combining the size and spacing of the basal obstacles into a roughness parameter, and relating it to the sliding velocity and basal shear stress. The small-scale roughness is thus included in a formulation influencing the large scale sliding of the glacier. In his theoretical derivation he assumed a bed with evenly distributed obstacles. If we assume now, that the size and spacing of the obstacles is not uniformly distributed in the entire model region, a locally varying description of the roughness can be useful.

**R2:** The effects of the bed topography on the flow are calculated by the model. To fit surface data the basal slipperiness distribution is then optimized. This optimized basal slipperiness distribution turns out to be spatially non-uniform because bed topography alone does not produce the observed spatial variations in surface velocity. The inverted basal slipperiness, needed by the numerical model for it to reproduce measured surface data, is therefore not due to some



variations in modelled bed topography. The slipperiness distribution is related to processes that are NOT accounted for by the modelled basal topography.

**Answer:** Yes, this is correct. Therefore again the interpretation of the basal roughness as a representation for a certain bed type is important. And the influences of the temperature and the basal water pressure have to be considered, which is done in the first approach.

**R2:** Since the 'roughness' estimates are based on the same topography data already included in the numerical model, then why would we expect these roughness estimates to give us added insight into the retrieved basal slipperiness distribution? This retrieved basal slipperiness distribution reflects aspects of the bed other than the geometry needed to fit the data (other than the geometry because it is already included). What these other aspects of the bed are is an open question (my guess is that they reflect spatial variations in till properties, basal water pressure, etc. etc.), but the point is that model does not need the spatial variations in basal slipperiness to mimic the effects of flow over its own bed geometry.

**Answer:** This we don't understand. The model results clearly show, that other factors are important, other than the glacier geometry, and thus bed shape, itself, to reproduce the surface flow structure. The question we are aiming to address is therefore what these other factors could be, how important they are and how they could be included in a formulation for basal sliding.

**R2:** I therefore don't fully understand why the authors try to relate inverted slipperiness with a roughness estimate of the bed they are already using in their model.

**Answer:** The roughness measure  $\xi$  we use does not directly represent the roughness as formulated in the original approach by Weertman. To use the roughness information anyhow, it is therefore necessary to translate the basal sliding parameter  $C_b$  to a meaningful range. For this the initial inversion step is needed.

**R2:** Now I'm open to the possibility that I may not have understood the paper correctly. If, for example, the basal roughness is estimated from a very high resolution (less than a fraction of ice thickness) area measurements of bed geometry, or if the resolution of the numerical model is not high enough to capture the known variations in basal topography on which the roughness estimates are based, then my criticism is invalid. But I do not know of any such high resolution measurements (measuring roughness along flight lines not aligned with flow and then interpolating between flight lines kilometres apart as done by Rippin et al is a futile exercise), and the resolution of the FE-mesh is clearly high enough to capture all spatial variations in existing compilations of PIG bed. I suggest giving the authors the chance to clarify the thinking behind their work and explain why comparing retrieved basal slipperiness with estimates of the 'roughness' of the bed, that are based on the same (or similar)

data set as they are using in their numerical model, is an interesting and important scientific question.

**Answer:** Estimates of basal roughness help us to try and say something about bed conditions and bed variability, and how these influence flow. Additionally the formulation of basal sliding in glacier modelling is still one of the most difficult questions to address; therefore inversion for basal parameters is the most commonly chosen approach. This approach, on the other hand, does not lead to a better understanding of the processes at the base. We therefore aim to combine information about the bed in a formulation of basal sliding.

We aim to reproduce the flow behaviour observed on a “real world” glacier and therefore understand the system better and make guesses about the underlying processes. This is different to assuming purely theoretical conditions and investigating specific processes, which can be clearly separated, like for example estimating the effect of roughness onto basal sliding. We believe that aiming to understand a “real world” glacier behaviour is an important scientific question to address.

**R2:** We should not forget that a sliding law is (to use an old phrase by Andrew Fowler) a matching condition between the inner and the outer flow. As such the sliding law represent processes not directly included or resolved by the model. For example processes happening on a spatial scale much smaller than those that can be resolved, or processes not included (regelation, cavitation, till deformation, etc. etc.). So for example in the old works by Nye, Kamb, Weertman, the focus was on how processes on small scales affect the bulk flow of ice. One of the questions was, for example, how one could replace a sinusoidal bed geometry with a flat one by changing the boundary conditions accordingly. Hence, the ‘roughness’ of the bed translates into a sliding law over another less rough bed. Comparing (inverted) sliding law parameters over a given bed with the roughness of the bed itself appears in this context questionable.

**Answer:** As the stress conditions in underlying substrate (hard bedrock or till) are not known, a jump condition for the momentum cannot be formulated. Instead a sliding relation often called a sliding law is required. We agree with the reviewer, that sliding relations that are applicable for this type of modelling study here, are approximating the sliding processes for a number of different reasons. First, these processes occur on a spatial scale much smaller than the model resolution. Second, not all the relevant processes themselves are implemented (e.g. heat transfer through the small obstacles required for regelation as in Weertman’s analysis of sliding). In addition, very little is known about the bed conditions for most areas in Antarctica and Greenland, e.g. if there exists sediment or hard bed rock, how thick the sediment layer is, how much water there is in the sediment or in the space between the ground and the ice or how mobile/resident the water is? Due to the pioneering work of Nye, Kamb, Weertman (mentioned by the reviewer, and we would like to add Lliboutry), we have now a better understanding of processes that are or might be important for basal motion (sliding + bed deformation). But their work is based on theoretical analyses for processes on a spatial scale that is up to now not accessible for

observations. One aim of our study is to bridge the gap between the processes on the sub-metre scale, the observed 'roughness' on the several-meter scale and the kilometre scale used in the numerical flow model. We think that every information available from observations should be used to constrain model parameters, if the processes must be parameterised for the stated reasons.

**R2:** p.s.

There is an additional point I would like to make that is just a general statement and does not directly relate to the submitted work but might be worthwhile to consider. The roughness used in Bingham and Siegert 2009, Rippin et al. 2011 appears very different from the one used by Nye and others in the late 60s and early 70s. It is unclear to me what the mathematical relationship between basal roughness, as defined by Siegert and others, and sliding over smooth bed really is. Has it been proved that sliding velocity increases monotonically with increasing roughness? And if the 'roughness' increases by, for example, a factor of 2, how does that affect sliding velocity? Will it increase or decrease?

**Answer:** We do not think that Bingham, Siegert and Rippin aim at answering this question. They do not try to derive a mathematical relationship between the roughness parameter they derive and velocity. Additionally it seems to be acceptable to use the term 'roughness' to describe bed variability, as this is what they are investigating. They use it more as a qualification of bed type and make guesses about the long-term structure of glacier flow. However, this should be answered by the according authors.

However, the reviewer points to a number of interesting questions, like the one if the sliding velocity increases with roughness. Results of the ISMIP-HOM experiment A, which simulates sliding over a bumpy bed (Pattyn et al., 2008) showed that the surface velocity decreases significantly with increased roughness - at least in the isothermal case. Our model results presented here agree with this finding. So far we cannot say how important strain-heating could be for a very rough bed and if this additional heat source could lead to a significant softer material at the base.

**R2:** I know that the expectation is that sliding velocity will decrease with increasing roughness, but that assumes roughness has been defined in a sensible way. I can't see anything in the Rippin or Bingham and Siegert papers to support this.

This may be a bit surprising statement on my behalf but even if one calls something roughness it does not mean that it is a useful or even a meaningful definition of roughness in terms of glacier motion. I suggest re-reading these papers on 'roughness' and while doing so replacing the word 'roughness' with some non-descriptive and less suggestive term. For example by replacing 'roughness' with 'hohu' (just some made up non-descriptive word). The question then becomes if and how 'hohu' affects basal sliding velocities. For 'hohu' to be a useful quantity this needs to be not only proven but quantified in detail as was done in the old works by Nye, Kamp, etc. (using a different definition of roughness) and then extended using various numerical and

analytical methods by Fowler, Meyssonier, Gudmundsson, Schoof, and Gagliardini, to name only a few. Unless this is done, there is no reason to expect the 'roughness' (or the hohu) as defined by Bingham and Siegert, and others, to be of any particular relevance to glacier flow.

**Answer:** The reviewer is right in expressing that the definition of roughness in the original sliding law by Weertman and the roughness we can observe today underneath ice sheets is on completely different horizontal and vertical scales. However, even decades after the first introduction of the sliding law and decades after technological development, there is no means to survey the roughness required for the sliding law on an adequate scale.

Last but not least, one has to keep in mind, that ice modelling requires a basal boundary condition for the momentum balance equation. As there is no information available on the stress inside the lithosphere and hence the jump condition does not lead any further, the sliding law serves as a dynamical boundary condition – in all ice sheet models, not only in ours. Using a sliding law is thus not only a pragmatic, but the only approach we can do today, although we hope that the next decade will lead to new insights of how to treat the basal boundary condition more realistic.

Therefore, we think that our treatment of the basal sliding law is an enhancement to many previous modelling studies, where often the parameters of the sliding law are simply tuned to match surface velocities. Whether we call the parameter roughness, local geometry variation or hohu doesn't really matter – although we think that the link between  $\xi$  and the term roughness is not too bad. To deal with the terminology roughness adequately, one would need to treat it scale dependent.

**Article (ISMIPHOM\_2008)**

Pattyn, F.; Perichon, L.; Aschwanden, A.; Breuer, B.; de Smedt, B.; Gagliardini, O.; Gudmundsson, G. H.; Hindmarsh, R. C. A.; Hubbard, A.; Johnson, J. V.; Kleiner, T.; Konovalov, Y.; Martin, C.; Payne, A. J.; Pollard, D.; Price, S.; Rückamp, M.; Saito, F.; Souček, O.; Sugiyama, S. & Zwinger, T.

Benchmark experiments for higher-order and full-Stokes ice sheet models (ISMIP-HOM)

*The Cryosphere*, **2008**, 2, 95-108

Manuscript prepared for The Cryosphere Discuss.  
with version 2014/07/29 7.12 Copernicus papers of the L<sup>A</sup>T<sub>E</sub>X class copernicus.cls.  
Date: 17 December 2014

# Thermal structure and basal sliding parametrisation at Pine Island Glacier - a 3D full-Stokes model study

**N. Wilkens<sup>1,2</sup>, J. Behrens<sup>3</sup>, T. Kleiner<sup>2</sup>, D. Ripplin<sup>4</sup>, M. Rückamp<sup>2</sup>, and A. Humbert<sup>2,5</sup>**

<sup>1</sup>Institute for Geophysics, University of Hamburg, Germany

<sup>2</sup>Alfred Wegener Institute, Helmholtz Centre for Polar and Marine Research, Bremerhaven, Germany

<sup>3</sup>Numerical Methods in Geosciences, University of Hamburg, Germany

<sup>4</sup>Environment Department, University of York, Heslington, UK

<sup>5</sup>Department of Geosciences, University of Bremen, Germany

Correspondence to: Nina Wilkens (nina.wilkens@zmaw.de)

## Abstract

Pine Island Glacier is one of the fastest changing glaciers in the Antarctic Ice Sheet and therefore in scientific focus. The glacier holds enough ice to raise global sea level significantly ( $\sim 0.5$  m), when fully melted. The question addressed by numerous modelling studies of the glacier focusses on whether the observed changes are a start for an uncontrolled and accelerating retreat. The movement of the glacier is, in the fast flowing areas, dominated by basal motion. In modelling studies the parametrisation of the basal motion is therefore crucial. Inversion methods are commonly applied to reproduce the complex surface flow structure at Pine Island Glacier, which use information of the observed surface velocity field, to constrain, among other things, basal sliding. We introduce two different approaches of combining a physical parameter, the basal roughness, with basal sliding parametrisations. This way basal sliding is connected again closer to its original formulation. We show that the basal roughness is an important and helpful parameter to consider and that many features of the flow structure ~~could~~ can be reproduced with these approaches.

## 1 Introduction

In the past decades the fastest changes in ice flow velocity, ice thickness and grounding line retreat in the Antarctic Ice Sheet have been observed in the region of Pine Island Glacier (PIG), Amundsen Sea Embayment, West Antarctica (Rignot, 2008; Wingham et al., 2009; Rignot, 1998; Joughin et al., 2010; Park et al., 2013). Additionally, the currently observed mass loss from the Antarctic Ice Sheet is also concentrated in the area around PIG (Horwath and Dietrich, 2009; Shepherd et al., 2012). Thus PIG shows an increased contribution to global sea level rise (Mouginot et al., 2014).

The bed below PIG lies below sea level in large areas, making it part of a so called marine ice sheet. In combination with a retrograde bed, which slopes down from the ocean towards the center of the glacier, this setting was postulated to be intrinsically unstable, via the so called "Marine Ice Sheet Instability" hypothesis (Hughes, 1973). This hypothesis is still up

for debate (Vaughan, 2008; Gudmundsson et al., 2012), while the trigger for the changes is thought to be enhanced ocean melting of the ice shelf (Dutrieux et al., 2014).

The dynamics of PIG are crucial for its future behaviour and therefore for its contribution to sea level rise. An important tool for investigating glacier dynamics are numerical ice flow models. Ice flow models simulate the flow of glacier ice, which is due to a combination of internal deformation and basal motion. ~~Dependent~~ Depending on the subglacial setting, basal motion can dominate the overall motion of a glacier, which is also the case for large areas of PIG. The parametrisation of basal motion in ice flow models is therefore important for the overall dynamics of a glacier. On the other hand the difficulty of observing basal properties renders the parametrisation one of the most challenging parts in ice flow modelling. In the absence of information on basal properties like bed type, structure and availability of liquid water, control methods are applied to simulate a complex glacier flow pattern, as present at PIG (e.g. MacAyeal, 1992; Joughin et al., 2009, 2010; Morlighem et al., 2010; Favier et al., 2014). These methods use the measured surface velocity field to invert for basal properties or effective viscosity and to adjust basal sliding parameters. Depending on the focus of the study, these approaches can provide important insights into glacier dynamics.

Due to the fast changes observed at PIG, a variety of modelling studies have been conducted on it. These studies address questions focusing on the sensitivity to changes in external conditions (ice shelf buttressing, basal conditions) (e.g. Schmelz et al., 2002) and on the contribution to future sea level rise (e.g. Joughin et al., 2010). The overarching question is, if the system will stabilise again in the near future, or if retreat might even accelerate (e.g. Katz and Worster, 2010; Gladstone et al., 2012; Favier et al., 2014; Seroussi et al., 2014).

The question whether the system will stabilise again in the future is an important one to address. Nonetheless in modelling studies one needs to simplify things, being forced to focus on certain processes and neglect others. The prognostic studies on PIG all use control methods to constrain basal sliding. Thus they define a spatially varying basal sliding parameter for the present flow state, and keep it constant during the prognostic simulations.

This way the basal sliding system is somehow decoupled from the rest of the system. Changes in basal conditions, by for example ~~grounding line migration (Park et al., 2013)~~, subglacial erosion (Smith et al., 2012; Rippin et al., 2014) or dynamic hydraulic systems, can not be considered with this approach. However, the basal sliding behaviour might be the crucial process to cause a further retreat or halt of the system. Gudmundsson et al. (2012) show that stable grounding line positions can be found on a retrograde bed, using models with 2 horizontal dimensions. We believe the basal sliding behaviour is a similarly important process as is the lateral buttressing. Therefore we focus on basal sliding parametrisations that consider ~~physical properties~~. measured basal roughness distributions. This accessible bed information could be in further steps combined with for example a time-dependent hydrological model, to consider changing basal conditions for the sliding behaviour of the glacier.

Here we present results of the thermo-mechanical 3D full-Stokes model COMice (implemented in the COMmercial finite element SOLver COMSOL Multiphysics<sup>®</sup>, cf. Pattyn et al. (2013); Wilkens (2014)), applied diagnostically to PIG. Initially we conduct a diagnostic inversion for a basal sliding parameter, as done in previous studies, to generate a reference simulation and analyse the thermal structure of the glacier. Since the inversion for basal sliding parameters is not sufficient for the physical understanding of basal motion, we introduce and test in a second step two methods of connecting ~~measured basal properties~~ basal roughness measures to the parametrisation of basal sliding and therefore constrain basal sliding with physically justified assumptions. Additionally we couple the sliding behaviour to the basal temperature, adding another physically based constraint. The first method matches a ~~single parameter~~ single-parameter basal roughness measure for PIG (~~Rippin et al., 2011~~), as presented in Rippin et al. (2011), onto a basal sliding parameter. The second method is based on ideas from Li et al. (2010), ~~using a two-parameter~~ where we use a two-parameter basal roughness measure, especially calculated for this study, to connect basal roughness to basal sliding ~~and is extended to be applied to PIG~~. The results are subsequently analysed and discussed.



## 2 The numerical flow model

### 2.1 Governing equations

The governing equations for the thermo-mechanical ice flow model COMice are the fluid dynamical balance equations, together with a formulation for the non-Newtonian rheology of ice. The balance equations are set up for mass, momentum and energy, and solved for the velocity vector  $\mathbf{u}$ , the pressure  $p$  and the temperature  $T$ .

The mass balance equation is given in case of incompressibility as

$$\operatorname{div} \mathbf{u} = 0. \quad (1)$$

The momentum balance equation is the Stokes equation, given by

$$\operatorname{div} \boldsymbol{\sigma} = -\rho_i \mathbf{g}, \quad (2)$$

with the Cauchy stress tensor  $\boldsymbol{\sigma}$ , the density of ice  $\rho_i$  and the acceleration of gravity  $\mathbf{g} = (0, 0, -g)^T$ . The stress tensor  $\boldsymbol{\sigma}$  is split into a velocity dependent part  $\boldsymbol{\tau}$ , the deviatoric stress, and a pressure dependent part  $p\mathbf{I}$ , with the identity matrix  $\mathbf{I}$ , such that  $\boldsymbol{\sigma} = \boldsymbol{\tau} - p\mathbf{I}$ . For incompressible materials only the deviatoric stress  $\boldsymbol{\tau}$  can result in strains, and is thus related to the velocity field  $\mathbf{u}$ , [via the strain-rate tensor  \$\dot{\boldsymbol{\epsilon}}\$  and the ice viscosity  \$\mu\$](#) , such that  $\boldsymbol{\tau} = 2\mu\dot{\boldsymbol{\epsilon}}$ . The strain-rate tensor  $\dot{\boldsymbol{\epsilon}}$  is given in components as

$$\dot{\epsilon}_{ij} = \frac{1}{2} \left( \frac{\partial u_i}{\partial x_j} + \frac{\partial u_j}{\partial x_i} \right),$$

in relation to Cartesian basis vectors. The ice viscosity  $\mu$  is described with use of Glen's flow law (Glen, 1955; Nye, 1957), such that

$$\mu(T', \dot{\boldsymbol{\epsilon}}_e) = \frac{1}{2} [A(T')]^{-1/n} \dot{\boldsymbol{\epsilon}}_e^{\frac{1-n}{n}}, \quad (3)$$

with the rate factor  $A(T')$ , the stress exponent  $n$  and the effective strain rate

$$\dot{\epsilon}_e = \sqrt{\frac{1}{2} \text{tr}(\dot{\epsilon}^2)}, \quad (4)$$

which is a scalar invariant of the strain-rate tensor  $\dot{\epsilon}$ . The viscosity  $\mu$  depends on the homologous temperature  $T'$  and the effective strain rate  $\dot{\epsilon}_e$ . The homologous temperature  $T'$  is the temperature relative to the pressure melting point  $T_{\text{pmp}}$ , defined as

$$T' = T + \beta_c p, \quad (5)$$

with the Clausius-Clapeyron constant  $\beta_c$ .

The pressure melting point  $T_{\text{pmp}}$  is described for typical pressures in ice sheets ( $p \lesssim 50$  MPa) by a linear relation, such that

$$T_{\text{pmp}} = T_0 - \beta_c p, \quad (6)$$

with the melting point at low pressures  $T_0$ .

The rate factor  $A(T')$  parametrises the influence of the temperature and the pressure ~~on the viscosity onto the viscosity~~  $\mu$  and is described by  $A(T') = A_0 e^{-Q/RT'}$  (Greve and Blatter, 2009), with a pre-exponential constant  $A_0$ , the activation energy for creep  $Q$  and the gas constant  $R$ . ~~To achieve a continuous function for  $A$  with a stress exponent  $n=3$ ; the suggested values for  $A_0$  and  $Q$  are taken from Paterson (1994).~~

The energy balance equation is given as

$$\rho c_p(T) \left( \frac{\partial T}{\partial t} + \mathbf{u} \cdot \text{grad } T \right) = \text{div}(\kappa(T) \text{ grad } T) + \psi, \quad (7)$$

with the thermal conductivity  $\kappa(T)$ , the specific heat capacity  $c_p(T)$  and an internal heat source term  $\psi = 4\mu\dot{\epsilon}_e^2$ , which connects mechanical and thermal energy.

The scalar values for all parameters used throughout this study are listed in Table 1.

## 2.2 Boundary conditions

The balance equations are defined under the assumption that the thermodynamic fields are sufficiently smooth, thus continuously differentiable, which is only the case for the inner parts of the glacier. The outer boundaries need specifically formulated boundary conditions. The vertical boundaries are the upper surface  $z_s$  and the base  $z_b$  of the glacier. The lateral boundaries are given by the ice divide, an inflow area and the calving front, indicated in Fig. 1. The grounding line indicates the change of the basal boundary conditions from grounded to floating ice.

### 2.2.1 Mass

Since the model is applied in a diagnostic manner and therefore the geometry is fixed, only the ice base  $z_b$  needs a kinematic boundary condition, to prevent the flow to point into the ground, and is given as  $\mathbf{u} \cdot \mathbf{n} = 0$ , with the unit normal vector  $\mathbf{n}$  pointing outwards from the surface. This formulation is applied to the entire ice base  $z_b$ , including grounded and floating parts, and also implies that no basal melting is considered.

### 2.2.2 StokesStress

The ~~boundary condition for the~~ upper surface  $z_s$  can be ~~derived~~ seen to be traction free by assuming that wind stress and atmospheric pressure are negligible compared to the typical stresses in the ice sheet. ~~The surface can therefore be assumed to be traction free, which implies, such~~ that  $\boldsymbol{\sigma} \cdot \mathbf{n} = 0$ .

~~The boundary condition for~~ At the base of the ~~ice shelf is based on the assumption that the floating ice shelf~~ shear stress induced by circulating sea water can be neglected (Weis et al., 1999) and the only stress onto the ice is exerted by the water. As the ice shelf floats it is assumed to fulfil the floating condition and the stress applied equals the stress of the displaced water column (Greve and Blatter, 2009), such that  $\boldsymbol{\sigma} \cdot \mathbf{n} = -\rho_{sw} g (z_{sl} - z_b) \cdot \mathbf{n}$ , with the density of sea water  $\rho_{sw}$  and the mean sea level  $z_{sl}$ .

25 For the boundary condition of the grounded ice, it is assumed that the stress vector  $\boldsymbol{\sigma} \cdot \mathbf{n}$  is continuous across the interface, such that  $\boldsymbol{\sigma} \cdot \mathbf{n} = \boldsymbol{\sigma}_{\text{lith}} \cdot \mathbf{n}$ , with the Cauchy stress tensor of the lithosphere  $\boldsymbol{\sigma}_{\text{lith}}$ . Since this tensor is not known, the condition has to be approximated. To do so, the basal stress vector  $\boldsymbol{\sigma} \cdot \mathbf{n}$  is split into its normal component  $N_b$  and its tangential component  $\tau_b$ . The basal normal stress  $N_b$  is a vector of the form  $N_b = -N_b \mathbf{n}$ . The overburden pressure of the ice is reduced in marine parts by the uplifting water pressure (Huybrechts, 1992), such that

$$N_b = \begin{cases} \rho_i g H & \text{for } z_b \geq z_{sl} \\ \rho_i g H + \rho_{sw} g z_b & \text{for } z_b < z_{sl}. \end{cases}$$

The assumptions made above imply a hydrology network which is perfectly connected to the ocean. This assumption is plausible near the grounding line, but becomes highly speculative towards the marine regions further inland. An additional hydrological model would be needed to realistically simulate the effective basal pressure, but is beyond the scope of this study. Even though more sophisticated parametrisations for the effective pressure exist (e.g. Leguy et al. (2014)), we stick with the strong assumption stated above, as water is likely present below all fast-flowing parts of PIG (Smith et al., 2013), which coincide with the marine regions.

In most modelling studies a so called Weertman-type sliding law is applied for the tangential component. This sliding law was originally developed by Weertman (1957) on the basis of two actual physical processes that take place, namely regelation and enhanced creep. An additional bed-separation index  $\tau_b/N_b$  (Bindschadler, 1983) and a temperature function  $f(T)$ , that controls submelt sliding, extend the Weertman-type sliding law to the form used here. It relates the basal sliding velocity  $\mathbf{u}_b = (\mathbf{u} \cdot \mathbf{t}_x, \mathbf{u} \cdot \mathbf{t}_y)^T$ , with the unit tangential vectors  $\mathbf{t}_x$  in the xz-plane and  $\mathbf{t}_y$  in the yz-plane, to the basal drag  $\tau_b = ((\boldsymbol{\sigma} \cdot \mathbf{n}) \cdot \mathbf{t}_x, (\boldsymbol{\sigma} \cdot \mathbf{n}) \cdot \mathbf{t}_y)^T$  and the basal normal stress  $N_b$  via a power law. In its simplest form it can be written as a linear connection, such that

$$25 \quad \mathbf{u}_b = C_b |\tau_b|^{p-1} N_b^{-q} f(T)_b = F \beta^2 \mathbf{u}_{bb}, \quad (8)$$

whereby  $C_b$  is originally seen as a roughness parameter,  $p$  and  $q$  are basal sliding exponents,  $N_b$  is related to the basal normal stress, defined in Eq. (15).

Sliding can occur at temperatures below the pressure melting point, as found by Fowler (1986). Therefore, we chose a temperature function  $f(T)$  that reflects this mechanism. Budd and Jenson (1989) used an exponential function for the temperature dependence of sliding by

$$f(T) = e^{\nu(T-T_{\text{pmp}})},$$

with a submelt sliding parameter  $\nu$  where  $\beta^2$  is a basal sliding parameter including all factors influencing the basal sliding behaviour other than the linear connection to basal stress. A more detailed description of sliding laws can be found in Sect. 3.2, as they are of central interest for this study.

Ice divides can be seen as mirror points where the direction of the driving stress and flow on one side of the divide opposes that of the other side. No flow across the ice divide is allowed, the tangential stresses vanish and therefore the boundary condition for ice divides is given by

$$\mathbf{u} \cdot \mathbf{n} = 0 \quad , \quad (\boldsymbol{\sigma} \cdot \mathbf{n}) \cdot \mathbf{t}_x = 0 \quad \text{and} \quad (\boldsymbol{\sigma} \cdot \mathbf{n}) \cdot \mathbf{t}_y = 0. \quad (9)$$

The boundary condition at the calving front is given by

$$\boldsymbol{\sigma} \cdot \mathbf{n} = -p_{\text{sw}} \mathbf{n}, \quad (10)$$

with the water pressure  $p_{\text{sw}}$  defined as

$$p_{\text{sw}} = \begin{cases} 0 & \text{for } z \geq z_{\text{sl}} \\ \rho_{\text{sw}} g (z_{\text{sl}} - z) & \text{for } z < z_{\text{sl}}. \end{cases} \quad (11)$$

The boundary condition for the inflow region is given as a Dirichlet condition by an inflow velocity field defined with the Shallow Ice Approximation (Hutter, 1983; Morland, 1984).

### 2.2.3 Temperature

The boundary conditions for the upper surface  $z_s$  and the ice shelf base (the floating part of  $z_b$ ), which is only given by Dirichlet conditions in prescribing the average annual surface temperature  $T_s(x, y, t)$  and the freezing temperature of seawater  $T_{sw}$ , respectively.

At the base of the grounded ice the boundary condition has to be formulated as a Neumann condition and the temperature gradient is prescribed as

$$\text{grad} T \cdot \mathbf{n} = \frac{q_{\text{geo}} + q_{\text{fric}}}{\kappa(T)}, \quad (12)$$

with the geothermal heat flux  $q_{\text{geo}}$  and the friction heating term  $q_{\text{fric}} = \mathbf{u}_b \cdot \boldsymbol{\tau}_b$  (Pattyn, 2003). This condition is only valid as long as  $T \leq T_{\text{pmp}}$ . If the basal temperature  $T$  reaches the pressure melting point  $T_{\text{pmp}}$ , it has to be switched to a Dirichlet condition with  $T = T_{\text{pmp}}$ , as the ice can not become warmer.

The boundary condition for the ice divide and the calving front are based on the assumption that there is no temperature gradient across the surface. It can thus be written in form of a thermal insulation  $(\kappa(T) \text{grad} T) \cdot \mathbf{n} = 0$ .

Temperatures at the inflow boundary are prescribed by a linear profile  $T_{\text{lin}} = \frac{T_{\text{pmp}} - T_s}{z_s - z_b} (z_s - z) + T_s$ .

### 2.3 Implementation

The thermo-mechanically coupled 3D full-Stokes model COMIce is implemented in the COMmercial finite element SOLver COMSOL Multiphysics<sup>®</sup> (cf. Wilkens (2014) for implementation details).

The model has been successfully applied in the diagnostic tests in the MISMIP 3D model intercomparison project (Pattyn et al., 2013).

### 2.3.1 Ice flow model

The ice flow model solves for the the velocity vector  $\mathbf{u}$  and the pressure  $p$ . The Babuska-Brezzi condition requires for numerical stability, that the basis functions for  $p$  are of lower order than for  $\mathbf{u}$ . Therefore we use linear elements for  $p$  and quadratic elements for  $\mathbf{u}$  (P1+P2).

To the effective strain rate  $\dot{\epsilon}_e$  (Eq. (4)) a small value of  $10^{-30} \text{ s}^{-1}$  is added, to keep the term non-zero. Model experiments have shown, that this does not affect the overall results (Pattyn, 2003; Cornford et al., 2012).

The boundary conditions set in the ice flow model are the kinematic and dynamic ones stated in Sect. 2.2.2.1 and 2.2.2, respectively. The kinematic condition at the ice base is implemented as a weak constraint, ~~in contrast to a pointwise constraint, for stability reasons~~ for stability reasons. Weak constraints apply boundary conditions in an integral sense and are therefore not as strict. They stand in contrast to pointwise constraints, which force the nodal value to the constraint and can thus lead to numerical instability (COMSOL, 2012).

The ~~sliding law is implemented as the inverse form of basal stress vector is implemented consisting of its tangential part (Eq. (14), such that 8))~~ and a normal part, given by the effective normal stress  $N_b$  (Eq. (15)), further described in Sect. 3.2, such that

$$\boldsymbol{\sigma} \cdot \mathbf{n} = \underline{F_b^{-1} \beta^2} u_b \mathbf{t}_x + \underline{F_b^{-1} \beta^2} v_b \mathbf{t}_y - N_b \mathbf{n}_z, \quad (13)$$

with  $u_b = \mathbf{u} \cdot \mathbf{t}_x$  and  $v_b = \mathbf{u} \cdot \mathbf{t}_y$ .

To the outer wall of the ice rises a no slip condition is assigned, as they are implemented as holes in the geometry.

### 2.3.2 Thermal model

The temperature is ~~solved for discretized~~ with linear elements, with boundary conditions from Sect. 2.2.2.2.3.

To avoid numerical instabilities due to strong temperature advection, and thus to ensure that the element Péclet number is always  $< 1$ , we use consistent stabilization methods provided by COMSOL Multiphysics<sup>®</sup>. Equation 7 is solved using a Galerkin Least Square (GLS) formulation (Codina, 1998) in streamline direction and crosswind diffusion (Hauke and Hughes, 2000) to the streamline direction. The chosen stabilization methods add less numerical diffusion the closer the numerical solution comes to the exact solution (COMSOL, 2012).

All Dirichlet conditions for the thermal model are implemented as weak constraints, for stability reasons.

The Neumann condition for the temperature at the base  $z_b$  is implemented in a way, that a heat flux is prescribed, as long as  $T < (T_{b,max} - 0.01)$ . The expression  $T_{b,max}$  prescribes a spatially variable field that defines the maximal basal temperature allowed for a region ( $T_{pmp}$  for grounded areas,  $T_{sw}$  for floating areas). If  $T \geq (T_{b,max} - 0.01)$ , the heat flux is gradually reduced and turns zero when  $T = (T_{b,max} + 0.01)$ . This procedure ensures that the basal heat flux can not increase  $T_b$  above  $T_{b,max} + 0.01$ . The smoothing of the step function ensures numerical stability, which was not found with a sharp step.

### 2.3.3 Mesh

The small aspect ratio of PIG (ratio of vertical to horizontal extent  $\epsilon = H L^{-1} \approx 10^{-3}$ ) requires an unstructured finite element mesh, to

### 2.3.3 Mesh

To maximise the resolution while minimising the amount of elements, we use an unstructured finite element mesh, shown in Fig. 2.

The upper surface  $z_b - z_s$  is meshed first with triangles. The horizontal edge lengths are 5 – 500 m at the grounding line and the calving front, 50 – 1000 m at the inflow area and 100 – 2000 m at the rest of the outer boundary. The resulting 2D surface mesh is extruded through the glacier geometry with a total of 12 vertical layers, with the spacing everywhere. The thickness of the vertical layers varies only with ice thickness. The spacing between the



layers is refined towards the base. The ratio of the lowest to the upper most layer thickness is  $0.01/0.01$ , leading to a thickness of the lowest layer of about 5 m for a total ice thickness of 3000 m.

25 The final mesh consists of  $\sim 3.5 \times 10^5$  prism elements, which results in  $\sim 5 \times 10^6$  degrees of freedom (DOF), when solved for all variables.

### 2.3.4 Solver

~~We chose a direct solver, which was the most stable choice for our problem, although uncommon for such a high number of DOF's. All available iterative solvers did not run stable. The use of a direct solver was timely manageable. We use a direct segregated solver, which solves iteratively. For solving the nonlinear system, a direct segregated solver is used, which conducts a quasi-Newton iteration. It solves consecutively: first for the velocity vector  $u$  and the pressure  $p$ , and thereafter for the temperature  $T$ . This way the (COMSOL, 2012). This allows for reduced working memory usage can be reduced. As a convergence criterion we set a relative tolerance of  $1e-6$ , meaning that the execution terminates once the relative error (defined in Eq.(??)) is smaller than the relative tolerance value chosen.~~

10 ~~The relative error  $err$  is defined by the weighted Euclidean norm~~

$$err = \sqrt{\frac{1}{M} \sum_{j=1}^M \frac{1}{N_j} \sum_{i=1}^{N_j} \left( \frac{|E_{i,j}|}{W_{i,j}} \right)^2},$$

~~with  $M$  being the number of fields (variables solved for),  $N$  the number. For the remaining linear systems of equations the direct solver Pardiso (COMSOL (2012) and <http://www.pardiso-pro.com> last access: 9 December 2014) is applied. While uncommon for such large numbers of DOF's in field  $j$ ,  $W_{i,j} = \max(|U_{i,j}|, S_i)$  with  $U_{i,j}$  being the current approximation to the solution vector and  $S_i$  a pre-defined scale factor, and  $E_{i,j}$  the estimated error in this vector (COMSOL, 2012), it proved to be computationally viable and robust, since all available iterative solvers exposed instabilities on this problem.~~

### 2.3.5 Geometry and input data

20 The geometry of the model was built with a consistent set of surface elevation, ice thickness and bed topography on a 1 km grid, created by A. Le Brocq and kindly provided by her for this work. The data set represents the thickness distribution of PIG for the year 2005 and earlier. The ~~basis data A. Le Brocq used are for Le Brocq data are based on~~ the surface elevation ~~from Bamber et al. (2009), which combines satellite radar and laser measurements.~~ The data of Bamber et al. (2009) and the ice thickness data ~~is from of~~ Vaughan et al. (2006).

The grounding line position used is given by a combination of the positions in the MODIS Mosaic Of Antarctica (MOA, Bohlander and Scambos, 2007), corresponding to the years 2003/2004, the position in Rignot (1998), corresponding to 1996, and the position that gives  
5 the smoothest ice thickness join of the glacier geometry, assuming the floatation condition. The location of the ice rises pinning the ice shelf at present are detected on TerraSAR-X images from 2011, with assistance of interferograms from Rignot (2002). The surface temperature used here is on a 5 km grid compiled by Le Brocq et al. (2010) (ALBMAP v1), based on the temperature data described in Comiso (2000). We use the geothermal  
10 heat flux  $q_{geo}$  from 2012 (updated version of Fox Maule et al., 2005), because a variety of sensitivity tests showed, that other data sets lead to too high velocities in regions with no or little basal sliding. The observed surface velocity is taken from Rignot et al. (2011), shown in Fig. 1, and used to validate the reference simulation.

## 3 Methods: roughness data and sliding laws

15 The central focus of this study is to investigate how basal sliding and measured basal roughness could be connected in a formulation of a basal sliding law. We will therefore first describe the roughness data used throughout this study. Thereafter we will give an overview of the basal sliding laws used and elucidate their connection to basal properties.

### 3.1 Roughness data

20 In this study we use two different data sets of basal roughness measures, compiled for the base of PIG. The first one is the single-parameter roughness measure as presented in Rippin et al. (2011) (c.f. Fig. 4b therein). The second one is a two-parameter roughness measure calculated especially for this study along ideas from Li et al. (2010).

Both roughness measures are based on Fourier transformations (FT), which is a key technique to derive basal roughness. A FT can be used to transform any surface into a sum of several periodically undulated surfaces. This way the amplitude and spatial frequency of the undulations can be expressed. For theoretical dynamic studies characterising the roughness by FT works well. However, to show the spatial distribution of roughness, in a glaciological context, a single-parameter measure  $\xi$  was introduced (Hubbard et al., 2000; Taylor et al., 2001). The single-parameter roughness measure  $\xi$  is defined as the integral of the spectrum within a specified wavelength interval. This method represents the amplitude of the undulations, but information about the frequency is lost. For PIG the single-parameter roughness measure  $\xi$  was calculated by Rippin et al. (2011) from a RES data set generated in austral summer 2004/05 (Vaughan et al., 2006). It is the same data set the model geometry is based on (Sect. 2.3.5), still the roughness measure includes higher resolution information, as the derivation is based on along track sample spacing of the order of 30 m (cf. Rippin et al. (2011)). Both data sets are then gridded with 1 km spacing.

Li et al. (2010) introduce a two-parameter roughness measure that represents the amplitude  $\xi_2$  and frequency  $\eta_2$  of the undulations. They introduce an interpretation how different basal topographies with their geomorphic implications can be distinguished from patterns of  $\xi_2$  and  $\eta_2$ . The interpretation from Li et al. (2010) is based on ideas by Bingham and Siegert (2009), which give an interpretation for the single-parameter roughness. Rippin et al. (2014) extended the interpretation for the two-parameter roughness measure. The implications for PIG will be discussed below.

Because of the statistical meanings of  $\xi_2$  and  $\eta_2$ , they can be used as representatives for the vertical and horizontal length scales present at the base. To do so the integration interval for  $\{\xi_2, \eta_2\}$  should be in the metre-scale waveband (Li et al., 2010).

25 The two-parameter roughness measure for PIG was calculated for this study. The spatial resolution of the underlain data for PIG is 34 m. A moving window is calculated with ( $N = 5$ ,  $2^N = 32$ ), which is the minimum for  $N$  that should be used (e.g. Taylor et al., 2004). With a spatial resolution of 34 m this leads to a moving window length of 1088 m, which is in the metre-scale waveband required by Li et al. (2010), to be able to apply the data in a sliding relation. The received fields of  $\xi_2$  and  $\eta_2$  for PIG are shown in Fig. 3.

According to Li et al. (2010), different basal properties and related geomorphic implications can be distinguished from patterns of  $\xi_2$  and  $\eta_2$ . A marine setting with intensive deposition and fast and warm ice flow, as proposed for the central part of PIG, is characterised by low values of  $\xi_2$  and high values of  $\eta_2$ , thus low-amplitude, low-frequency roughness.

5 Here it has to be noted that the second parameter  $\eta_2$  should be more accurately seen as representing the wavelength of roughness, rather than the frequency, as high values correspond to low frequencies (Rippin et al., 2014). Nonetheless we continue here referring to  $\eta_2$  as the roughness frequency for consistency with Li et al. (2010).

10 The suspected low-amplitude, low-frequency roughness is not necessarily found in the central trunk area, as can be seen in Fig. 3. Instead it seems to be more dominated by low-amplitude, high-frequency roughness, which can, following Li et al. (2010), be interpreted as a continental setting after intensive erosion, also with fast and warm ice flow. Still, this interpretation can not be seen as a contradiction to the suspicion of the presence of marine sediments. It is important to state that absolute values of roughness cannot be derived from these calculations, but rather it is the patterns relating to relative roughness values that are significant.

### 15 3.2 Sliding laws

20 So called "Weertman-type sliding laws" are most commonly applied in modern modelling studies, for which the basis was established by Weertman (1957). He developed a mathematical description for the mechanisms that influence basal sliding. One focus lay hereby on connecting small scale processes with larger scale sliding effects. Nye (1969) and Kamb (1970) worked on related problems and they all found that the basal sliding velocity  $u_b$  varies with some

power of the basal shear stress  $\tau_b$ , depending on the dominant mechanism. Additionally they find that the basal sliding velocity  $u_b$  also sensitively depends on the roughness of the bed.

25 The processes considered by Weertman (1957), Nye (1969) and Kamb (1970) are only relevant for sliding over hard bedrock, where an upper limit for sliding velocities is found ( $u_b < 20 \text{ m a}^{-1}$  Cuffey and Paterson (2010)). For faster sliding velocities weak deformable substrate or water filled cavities have to be present. Water filled cavities reduce the contact between the ice and the bedrock, therefore effectively reducing the roughness of the bed and their effect can be considered via the basal normal stress  $N_b$ , also called effective pressure (Bindschadler, 1983).

5 Fast sliding velocities can only occur when the glacier base is at pressure melting point, but also below these temperatures some sliding can be present (Fowler, 1986). This mechanism can be reflected by a temperature function  $f(T)$ , which regulates sub-melt sliding.

Considering the above stated thoughts leads to a sliding law of the form

$$u_b = C_b |\tau_b|^{p-1} N_b^{-q} f(T) \tau_b = \frac{1}{\beta^2} \tau_b, \quad (14)$$

10 whereby  $C_b$  is originally seen as a roughness parameter,  $p$  and  $q$  are basal sliding exponents and  $N_b$  is related to the basal normal stress, defined in Eq. (15). When written in a linearised form, as already introduced in Sect. 2.2.2, all effects influencing the basal sliding velocity  $u_b$ , other than the linear relation to the basal shear stress  $\tau_b$ , are summarized in a basal sliding parameter  $\beta^2$ , which leads to a spatially varying field obtained by inversion techniques.

15 In the following we will further define the single components in the basal sliding law, as used throughout this study.

The basal normal stress  $N_b$  is a vector of the form  $N_b = -N_b n$ . The overburden pressure of the ice is reduced in marine parts by the uplifting water pressure (Huybrechts, 1992),

such that

$$N_b = \begin{cases} \rho_i g H & \text{for } z_b \geq z_{sl} \\ \rho_i g H + \rho_{sw} g z_b & \text{for } z_b < z_{sl}, \end{cases} \quad (15)$$

with the ice thickness  $H$ . The assumptions made above imply a hydrology network which is perfectly connected to the ocean. This assumption is plausible near the grounding line, but becomes highly speculative towards the marine regions further inland. An additional hydrological model would be needed to realistically simulate the effective basal pressure, but is beyond the scope of this study. Even though more sophisticated parametrisations for the effective pressure exist (e.g. Leguy et al. (2014)), we stick with the strong assumption stated above, as water is likely present below all fast flowing parts of PIG (Smith et al., 2013), which coincide with the marine regions.

The temperature function  $f(T)$  is taken as suggested by Budd and Jenssen (1987) as an exponential function, such that

$$f(T) = e^{\nu(T-T_{pmp})}, \quad (16)$$

with a submelt sliding parameter  $\nu$ .

The roughness parameter  $C_b$  will be related to the single-parameter roughness measure from Rippin et al. (2011) in Sect. 4.2, and described in detail there.

A different approach to describe basal sliding, and also considered in this study, is introduced by Li et al. (2010). It is based on Weertmans original formulation (Weertman, 1957) of describing the sliding mechanisms of regelation and enhanced creep, such that

$$u_b = C_W \left( \tau_b \frac{l^2}{a^2} \right)^{\frac{(1+n)}{2}}, \quad (17)$$

whereby  $C_W$  is a parameter defined by thermal and mechanical properties of the ice ( $C_W = 4.46$  in our example),  $l$  is the obstacle spacing,  $a$  the obstacle size (cf. Weertman (1957)) and  $n = 3$  the stress exponent.

Li et al. (2010) state that the two-parameter roughness measures  $\xi_2$  and  $\eta_2$ , representing the amplitude and frequency of the roughness (cf. Sect. 3.1), can be used as a proxy for the vertical and horizontal length scales present at the base, due to their statistical meanings, such that

$$a = c_1 \xi_2^{\frac{1}{2}} \quad \text{and} \quad l = c_2 \eta_2^{\frac{1}{2}},$$

with  $c_1$  and  $c_2$  being proportionality factors.

Entering this into Weertmans original formulation (Eq. (17)) and additionally including a temperature function  $f(T)$  as introduced above, leads to

$$u_b = C_L f(T) \left( \tau_b \frac{\eta_2}{\xi_2} \right)^{\frac{(n+1)}{2}}, \quad (18)$$

with the constant  $C_L = C_W (c_2/c_1)^{1+n}$ . As the proportionality factors  $c_1$  and  $c_2$  are not further defined, we take  $C_L$  as a single parameter to adjust.

## 4 Results

We conduct numerical simulations with the model COMice set up for the PIG region. First, in Sect. 4.1, a reference simulation is conducted, where measured surface velocities are inverted for basal sliding parameters, as is commonly done for modelling the flow of PIG (e.g. Joughin et al., 2009; Morlighem et al., 2010; Favier et al., 2014; Seroussi et al., 2014). This approach leads to a realistic surface flow structure, ~~but~~ and lets us analyse the thermal structure of the glacier. Nonetheless the approach is dissatisfying when aiming to constrain basal sliding with physical parameters at the base of the glacier. Therefore, in a second step, we introduce two approaches for the parametrisation of basal sliding that consider the basal roughness below the glacier in the formulation of a basal sliding law. The first approach, Sect. 4.2, is based on the Weertman-type sliding law as shown in Eq. (14) and considers

20 [the single-parameter roughness measure from Rippin et al. \(2011\)](#). The second approach, Sect. 4.3, is based on the idea of Li et al. (2010) to ~~connected-connect~~ basal sliding to ~~a two parameter roughness index~~. [the two-parameter roughness measure, introduced in Sect. 3.1.](#)

## 4.1 Reference Simulation

25 The main difficulty is to capture the distinct surface flow pattern, by making appropriate assumptions about the basal sliding behaviour. Many ice modelling studies use a constant set of basal sliding parameters to reproduce somewhat realistic surface velocity fields (e.g. Rückamp, 2011; Kleiner and Humbert, 2014). This approach can not be adopted for PIG, as it leads to a shut down of parts of the fast flowing main trunk, due to very low basal shear stresses in that region (Joughin et al., 2009; Morlighem et al., 2010). Instead, for our  
5 reference simulation, an inversion for basal parameters is conducted, as already done by previous studies (e.g. Joughin et al., 2009; Morlighem et al., 2010; Favier et al., 2014).

### 4.1.1 ~~Method~~Simulation procedure

The inversion method (cf. Schmelz et al., 2002) used for our reference simulation starts by assuming a linear sliding law of the form  $\tau_b = \beta^2 \mathbf{u}_b$  ([inverted version of Eq. \(14\)](#)), with  $\beta^2$   
10 being the basal sliding parameter to be inferred.

Additionally a simulation is conducted, where the glacier base is not allowed to slide. Therefore the resulting surface velocity field  $\mathbf{u}_{s,nosl}$  can be seen to be solely due to internal deformation. The basal sliding velocity  $\mathbf{u}_b$  can be approximated by subtracting the surface velocity due to internal deformation  $\mathbf{u}_{s,nosl}$  from the measured surface velocity field  $\mathbf{u}_{obs}$  :  
15 ~~The resulting basal drag~~ ([Rignot et al. \(2011\)](#), Fig. 1). [The basal drag from the simulation where no basal sliding is allowed](#)  $\tau_{b,nosl}$  is taken as a good first representative of the real basal drag distribution  $\tau_b$ . With this ~~,the~~ [the field of the](#) basal sliding parameter  $\beta^2$  is defined as

$$\beta^2 = |\tau_{b,nosl}| (|\mathbf{u}_{obs}| - |\mathbf{u}_{s,nosl}|)^{-1}, \quad (19)$$



20 shown in Fig. 4.

The basal sliding parameter  $\beta^2$  is subsequently applied in the forward model in the linear sliding law. Since the amount of internal deformation in the ice crucially depends on the ice temperature (Eq. (3)), it is important to consider a realistic temperature distribution within the ice. At this point it is important consider to note, that the model is applied in a diagnostic manner and therefore the received temperature distribution is a steady state one for a fixed geometry with constant boundary conditions, which might differ from the actual transient field. Nonetheless the received field is likely to show a better approximation to reality than simply assuming a certain distribution. To consider a realistic temperature distribution within the ice, we conducted conduct the above described procedure in an iterative manner. We first conducted conduct a “no sliding” simulation  $\text{nosl}, 1$ , with a constant temperature of  $T = 263.15\text{K}$ . The resulting surface velocity field  $u_{s,\text{nosl},1}$  and basal drag  $\tau_{b,\text{nosl},1}$  lead to a basal sliding parameter  $\beta_1^2$ . This basal sliding parameter  $\beta_1^2$  enters the simulation with basal sliding  $\text{s1}, 1$ , where the temperature field is now solved for as well. The thus found temperature distribution enters the next “no sliding” simulation  $\text{nosl}, 2$  as a constant field. Now again a basal sliding parameter  $\beta_2^2$  is found, entering the next simulation with basal sliding  $\text{s1}, 2$ , which is our final reference simulation, later referred to as  $\text{ref}$ . Thus the procedure is stopped after two iterations, and listed in a schematic manner as:  $\text{nosl}, 1(T = 263.15\text{K}) \rightarrow \beta_1^2 \rightarrow \text{s1}, 1(T \text{ solved}) \rightarrow \text{nosl}, 2(T \text{ from } \text{s1}, 1) \rightarrow \beta_2^2 \rightarrow \text{s1}, 2/\text{ref}(T \text{ solved})$ .

#### 4.1.2 Velocity field

The resulting surface velocity field from the reference simulation is shown in Fig. 5, together with an indication and numbering of the different tributaries, feeding into the fast flowing central stream. The numbering of the tributaries for tributaries 1-10 is based on Stenoien and Bentley (2000). The numbering used in Vaughan et al. (2006), Karlsson et al. (2009) and Rippin et al. (2011) is the same for the even numbers, but shifted by 1 for the odd numbers, as they missed tributary 1 from the numbering by Stenoien and Bentley (2000).

We extended the numbering from Stenoien and Bentley (2000) to the tributaries 11-14, which are entering the ice shelf.

The general pattern of the surface velocity field is well reproduced in the reference simulation, compared to the observed surface velocity field  $|u_{\text{obs}}|$  (Rignot et al., 2011, shown in Fig. 1). The tributaries are all in the right location and the velocity magnitudes agree in most areas well. The highest differences between  $|u_{\text{s,ref}}|$  and  $|u_{\text{obs}}|$  are found in the ice shelf, where the simulated velocities are up to  $1 \text{ km a}^{-1}$  smaller than the observed ones.

When solely looking at the velocity magnitudes, shown in Fig. 6, we again find that for higher velocities the simulated velocity field  $|u_{\text{s,ref}}|$  is lower than the observed field  $|u_{\text{obs}}|$ . The spread around the diagonal for lower velocities appears bigger, which is mainly due to the logarithmic axes chosen. For higher flow velocities the direction of flow of the simulated field agrees well to the direction of the observed field. This is shown as a colour code for the angle offset between the velocity vectors in Fig. 6. For slower velocities the angle offset is bigger, coinciding with a higher measurement error for slower velocities.

### 4.1.3 Temperature regime

Our simulations show, that under PIG large areas are at the pressure melting point  $T_{\text{pmp}}$ . This can be seen in Fig. 7, where the temperature relative to the pressure melting point at the base  $T'_{\text{b,ref}}$  (homologous temperature as given in Eq. (5)), **at the base**  $T'_{\text{b,ref}}$  is shown. In general the overall flow pattern is reflected in the basal temperature structure, with fast flowing areas being underlain by a temperate base. This can be seen with help of the location of the tributaries in Fig. 7.

Figure 8 shows the homologous temperature  $T'_{\text{ref}}$  at three vertical slices, of which the location is indicated in Fig. 7. The first slice shown in Fig. 8a) is located furthest away from the ice shelf, towards the inner parts of the glacier. Figures 7 and 8 show that the base is mainly temperate while the inner ice body, away from the base, is predominantly cold. A similar picture is found in the next slice, shown in Fig. 8b), which is located further downstream towards the ice shelf. Here, additionally a cold core can be seen, located in the fast flowing central stream (cf. Fig. 5). The next slice, shown in Fig. 8c), partly crosses the

20 ice shelf. It can be well observed that a cold core is entering the ice shelf. To the right of the ice shelf, approximately where tributary 11 is located (cf. Fig. 7), a small temperate layer is found.

## 4.2 Parametrisation 1: Relating the single-parameter roughness and measure $\xi$ to the basal sliding parameter $C_b$

### 25 4.2.1 Method Simulation procedure

From the results of the reference simulation, it could be suspected that different types of sliding conditions must be present below PIG. Instead of inverting for one spatially varying parameter, we now connect the basal sliding parameter  $C_b$  of Eq. (14) to the measured basal roughness  $\xi$  (Rippin et al., 2011), (Rippin et al. (2011), Sect. 3.1), as it is closest to the originally physical meaning of  $C_b$  (cf. Sect. 2.2.23.2).

5 In the following we will refer to the basal sliding parameter  $C_b$ , when it is related to the basal roughness measure  $\xi$  in this section as  $C_\xi$ . The absolute values of the roughness measure  $\xi$  are dependent on parameters chosen for its derivation. At the same time the sliding parameter  $C_b$  depends not only on mechanical properties, such as basal roughness, but also thermal properties. Therefore, the roughness measure  $\xi$  can not directly be used  
10 as the sliding parameter  $C_\xi$ .

To use the roughness information, we select a range for the sliding parameter  $C_b$ , obtained via the approximation

$$C_b = \frac{(|\mathbf{u}_{\text{obs}}| - |\mathbf{u}_{\text{s,nosl}}|) N_b^q}{|\boldsymbol{\tau}_{\text{b,nosl}}|^p}, \quad (20)$$

15 with the effective normal stress  $N_b$  (Eq. (15)) and  $p = 1$ . The basal sliding exponent  $q$  is taken as 0, 1 or 2, which regulates the effect of the effective normal stress onto the sliding velocities. The resulting logarithmic range is thereafter matched onto the normed and inverted distribution of the roughness measure  $\xi$ , referred to as  $\xi_n$ . It is inverted as lowest

roughness correlates with highest basal sliding and therefore highest values of  $C_\xi$ . This way we make sure to derive surface velocities within a realistic range.

20

We conduct 15 simulations, where each parameter combination represents a potential subglacial setting. In all simulations  $p = 1$ , while  $q$  is varied. Simulations 1-5 are conducted with  $q = 0$ , simulations 6-10 with  $q = 1$  and simulations 11-15 with  $q = 2$ . For the different values of  $q$ , the range of  $C_\xi$  is varied. The widest range of  $C_\xi$  consists of the maximum values found by approximation for  $C_b$  (Eq. (20)). [Exact values can be found in \(Wilkins, 2014\)](#).

25

## 4.2.2 Velocity field

The resulting surface velocity fields are analysed in a quantitative and qualitative manner. For the quantitative manner the root-mean-square (RMS) deviation  $\text{RMS}_{u_s}$  between the simulated and the reference surface velocity fields are analysed. The  $\text{RMS}_{u_s}$  is given by

$$5 \quad \text{RMS}_{u_s} = \sqrt{\frac{1}{m} \sum_{i=1}^m (|\mathbf{u}_{s,\text{sim}}|_i - |\mathbf{u}_{s,\text{ref}}|_i)^2}, \quad (21)$$

with  $m$  being the number of discrete values on a regular grid with 1 km spacing.

The surface flow field is additionally separated into three distinct regions of fast flow velocities ("Fast"), slower flow velocities ("Slow") and the entire model region ("All") (detailed description in Wilkins (2014)). The regions of all tributaries (1-14), the central stream (CS) and the shelf area (Shelf), as shown in Fig. 9b ~~and e~~ [and 9c](#), are combined to the region "Fast", while the remainder is the region "Slow".

10

15

Figure 9a ~~and e~~ shows the  $\text{RMS}_{u_s}$  for the regions "Fast", "Slow" and "All" between the simulated and the reference surface velocity fields. It can be seen, that the "Fast" regions differ most for all parameter combinations tested here. Additionally for the entire region "All" there seems to be no single parameter combination, that minimises the  $\text{RMS}_{u_s}$  value and therefore appropriately represents the basal conditions below PIG in a sliding law. Nonetheless some of the complex surface flow features could be reproduced with our approach, which

can only be seen by looking at the qualitative structure of the resulting surface flow fields. Figure 9b) shows the surface velocity field of simulation 2. The location of tributary 7 and the central stream are well reproduced.

Especially in the simulations 11-15, with  $(p, q) = (1, 2) q = 2$ , a much better representation of the central stream and the inflow into the ice shelf across the grounding line is found, as can be seen as an example in the surface flow field from simulation 11, shown in Fig. 9c). The influence of the effective pressure  $N_b$  is thus emphasised. At the same time this method does not lead to a full reproduction of the surface flow structure. This suggests that other processes, not considered here, are also important for the basal sliding behaviour. A possibility, not tested yet due to time constraints (for a detailed description of the solution time of the simulations refer to Wilkens (2014)), is the effect of the basal stress exponent  $p$ . Increasing it would possibly to some extent regulate the high velocities in some areas, due to low basal stresses.

### 4.2.3 Temperature regime

The basal homologous temperature from simulation 2, shown in Fig. 10, shows a very clear structure of the temperate base below the tributaries, even though they are not clearly visible in the flow field (cf. Fig. 9b). The temperature driven separation between tributaries 2 and 4 and tributaries 7 and 9 are even better visible than in the reference simulation (cf. Fig. 7). The structure of the basal homologous temperature of all other simulations look very similar to that of simulation 2, although the total area fraction of ice at pressure melting point varies, as well as the separation between the tributaries.

Another interesting feature found in the structure of the basal temperature from simulation 2 is the advection of warmer ice into the shelf. This feature can be attributed to the implementation of the thermal basal boundary condition in the shelf. While the heat flux is not allowed to raise the temperature above 271.15 K, it does not hinder the advection of warmer ice from the grounded areas.

The structure of the bands of warmer ice agree well with melt channels below the ice shelf as found by Vaughan et al. (2012).

## 4.3 Parametrisation 2: Li-sliding

### 4.3.1 Method

Another approach to relate the basal roughness to the basal sliding velocity was introduced by Li et al. (2010). We test their idea for applicability to PIG. Li et al. (2010) introduce a two-parameter roughness index two-parameter roughness measure that represents the amplitude  $\xi_2$  and frequency  $\eta_2$  of the undulations.

The two-parameter roughness index at PIG was calculated with a moving window length of 32 points ( $N = 5, 2^N = 32$ ), which is the minimum that should be used (e.g. Taylor et al. (2004)). With a spatial resolution of 34m, this leads to a moving window length of 1088m, which is in the metre-scale waveband required by Li et al. (2010), to be able to apply the data in a sliding relation. The thus-calculated roughness amplitude  $\xi_2$  and roughness frequency  $\eta_2$  are shown in Fig. 3. Because of the statistical meanings of  $\xi_2$  and  $\eta_2$ , they can be used as a proxy for the vertical and horizontal length scales present at the base.

Li et al. (2010) introduce a structure for delineating different basal topographies and their geomorphic implications from patterns of  $\xi_2$  and  $\eta_2$ , which is based on ideas by Bingham and Sieg extended by Rippin et al. (2014). According to this, a marine setting with intensive deposition and fast and warm ice flow, as proposed for the central part of PIG, is characterised by low values of  $\xi_2$  and high values of  $\eta_2$ , thus low-amplitude, low-frequency roughness. This is not necessarily the case for the central trunk area, as can be seen in Fig. 3. Instead it seems to be more dominated by low-amplitude, high-frequency roughness, which can be, following Li et al. (2010), interpreted as a continental setting after intensive erosion, also with fast and warm ice flow. Still, this interpretation can not be seen as a contradiction to the earlier stated suspicion of the presence of marine sediments. We only considered the relative relation of high and low values. Absolute values can not be taken here, as they always depend on the spatial resolution of the underlain data, the moving window length and other details for the derivation process of the roughness index. as described in Sect.

3.1.

By assuming, that the controlling obstacle size is dominating (cf. Weertman (1957)), Li et al. (2010) build on the idea of Weertman (1957) and relate the two parameter roughness index  $\{\xi_2, \eta_2\}$  to a basal sliding velocity, such that

$$u_b = c \left( \frac{\eta_2}{\xi_2} \right)^{\frac{(n+1)}{2}},$$

where  $c$  is a factor not dependent on geometrical conditions and  $n = 3$  is the stress exponent.

To be able to apply the above stated relation as a sliding law in our model, we relate the basal sliding velocity  $u_b$  to the basal shear stress  $\tau_b$ , by considering the original approach by Weertman (1957), such that

$$u_b = C_L \left( \tau_b \frac{\eta_2}{\xi_2} \right)^{\frac{(n+1)}{2}},$$

with the constant  $C_L = C_W (c_2/c_1)^{1+n}$ . The value for  $C_W$  can be estimated (Weertman, 1957), and is in our example about  $C_W = 4.46 \times 10^{-29} \text{m}^3 \text{s}^3 \text{kg}^{-2}$ . The proportionality factors  $c_1$  and  $c_2$  on the other hand are not further defined. Therefore we take  $C_L$  as a single parameter to adjust.

For all simulations conducted in this section, only the ice flow model is solved for, due to time constraints (e. f. cf. Wilkens (2014)). The temperature distribution within the ice is taken from the reference simulation. The base below the fast flowing areas is thus temperate in all simulations (cf. Fig. 7). Use of the temperature field from the reference simulation gives the opportunity to further expand the approach from Li et al. (2010) and connect the sliding behaviour to the basal temperature, thus only allowing ice to slide where  $T$  is close to  $T_{\text{pmp}}$ . This was already done in the reference simulation (cf. Sect. 4.1) and the simulations with Parametrisation 1 (cf. Sect. 4.2), but is new to the approach by Li et al. (2010). Thus the basal sliding law now contains the temperature function  $f(T)$  (cf. Eq. (16)), such that the

basal boundary condition is given as-

$$\tau_b = \left( \frac{u_b}{C_L f(T)} \right)^{\frac{2}{(n+1)}} \left( \frac{\xi_2}{\eta_2} \right).$$

The use of the temperature function  $f(T)$  slightly reduces the RMS error of the simulated surface velocity field to that of the reference simulation ~~shown below~~, but does not change the overall picture, as achieved without the use of  $f(T)$ .

### 4.3.2 Velocity field

~~The simulations we conduct vary over~~ We conduct 18 simulations, whereby the value of  $C_L$  (Eq. (18)) is varied in the range  $[3 \times 10^{-2}; 3 \times 10^2]$   $\text{Pa}^{-2} \text{m a}^{-1}$ .

### 5 4.3.2 Velocity field

The  $\text{RMS}_{u_s}$  deviations between the reference and simulated results are shown for all simulations in Fig. 11a), and show a somewhat regular pattern. For the slower flowing areas, the  $\text{RMS}_{u_s}$  value increases with increasing  $C_L$ . For the faster flowing areas, the  $\text{RMS}_{u_s}$  value first slightly decreases with increasing  $C_L$ , and, after reaching a minimum of  $\text{RMS}_{u_s} = 500 \text{ m a}^{-1}$  for  $C_L = 1.58 \text{ Pa}^{-2} \text{ m a}^{-1}$ , increases with increasing  $C_L$ . Since we conduct simulations with discrete values for  $C_L$ , the value of  $\text{RMS}_{u_s} = 500 \text{ m a}^{-1}$  represents the minimum value for the simulations conducted here, and not an absolute minimum. The  $\text{RMS}_{u_s}$  value for the entire region "All", shows a similar behaviour of first decreasing and then increasing with increasing  $C_L$ , with a minimum  $\text{RMS}_{u_s}$  value of  $271 \text{ m a}^{-1}$  for  $C_L = 1 \text{ Pa}^{-2} \text{ m a}^{-1}$ .

When looking at the structure of the resulting surface flow fields, shown in Fig. 11b) ~~and c) and 11c~~, it is apparent that some features of the observed surface flow field are reproduced. The central stream in all the simulations from this section is partitioned into a faster flowing upper part, and a slower flowing lower part, in the vicinity of the ice shelf.

No single value for  $C_L$  could be found, that reproduces the surface velocity field of PIG with all its features. For higher  $C_L$  values, that reproduce the velocities in the central stream



in a better manner, the velocities in the slower flowing area around tributaries 3, 5, 7 and 9, located to the South of the main stream, are simulated much too high. Additionally, the area around tributary 14 behaves slightly different to most other tributaries. It speeds up much faster for much lower values of  $C_L$ . This is related to the low roughness measures  $\xi_2$  and  $\eta_2$  in that region.

## 5 Discussion

We have shown that the complex surface flow structure of PIG could be well reproduced with our simplified approach of an inversion for a basal sliding parameter  $\beta^2$ . Although the simulated flow pattern agrees well with observations, some differences in the magnitude of the surface flow velocities were found. These differences are highest in the ice shelf, and might be partly related to a slower inflow from the grounded areas. The simulated velocity is about  $1 \text{ km a}^{-1}$  slower than the observed surface velocity just before the grounding line in flow direction. This might be due to the position of the grounding line in our model. The grounding line position in our model is further downstream than the location in 2009, to which the observed surface velocity field belongs (2007-2009). Or it might be caused by the method of inferring  $\beta^2$ , as  $\tau_{b, \text{nosl}}$  is not vanishing near the grounding line, as would be expected (compare to Joughin et al. (2010); Morlighem et al. (2010)).

The main cause though seems to be that we did not account for the highly rifted shear margins in our model. These shear margins have been shown to be rheologically softer than undamaged ice (e.g. Humbert et al., 2009). In reality the shear margins partly uncouple the fast flowing central part from the surrounding ice. In our model we treat the shear margins rheologically equal to undamaged ice. This leads to an overestimation of the flow outside the central stream, and an underestimation within the central stream in the main trunk. The softening due to shear margins can be included in different ways, as for example done in Joughin et al. (2010); Favier et al. (2014), and will be included in future model versions.

The use of our high resolution thermo-mechanical full-Stokes model COMICE further allowed for an analysis of the thermal structure of the glacier. We found the base of the glacier

20 to be predominantly temperate, especially the fast flowing areas, while the rest of the inner ice body is mainly cold. This finding is consistent with the general definition of an Antarctic glacier, where, due to cold conditions at the surface, the cold-temperate transition surface (CTS) (Blatter and Hutter, 1991) is located at or near the base. To form a significant basal temperate layer Blatter and Hutter (1991) find that strain heating is the necessary or dominant mechanism. This also agrees well with our results, as the flow of PIG is dominated by basal sliding and therefore strain heating due to internal deformation is small. Only an area around tributary 11 (cf. Fig. 7 and 8c), where strain heating is much higher, shows the existence of a somewhat larger temperate layer at the base.

Unfortunately there are no measured temperature profiles available at PIG, to which our results could be compared. Nonetheless our findings of a temperate base below some parts of PIG are supported by findings from Smith et al. (2013), who find hints for the existence of water below the glacier.

As the first new parametrisation for basal sliding we tested the applicability of including actual measured roughness data in a sliding law, to reproduce the surface flow field structure of PIG. As a motivation we use the original ideas that motivated the Weertman-type sliding law, as shown in Eq. (14), and that relate the basal sliding parameter  $C_b$  to the basal roughness  $\xi$  (Rippin et al., 2011). We combine the spatial distribution of the basal roughness  $\xi$  with a plausible range of the basal sliding parameter  $C_b$ , to create a new basal sliding parameter  $C_\xi$ . This new parameter  $C_\xi$  is applied in the basal sliding law in different forms. On the one hand the range of values for  $C_\xi$ , on the other hand the influence of the effective pressure  $N_b$  in the sliding law is varied. The variation of the range for  $C_\xi$  is done to test the influence of the extreme values onto the flow field. The increase of the influence of the effective pressure  $N_b$  is done to investigate the importance of the marine setting, as large parts below the glacier are below sea level.

We find that the location of many tributaries can be reproduced with this approach, although not the full complexity of the flow structure. The central stream is in large areas underlain by a very smooth bed, which becomes rougher towards the grounding line. We have shown ~~that~~ with this approach, for a fast transition across the grounding line, the

20 influence of the effective normal stress  $N_b$  onto basal sliding must be large in that area. The low effective normal stress in that area leads to higher basal sliding velocities. This is especially plausible in the vicinity of the grounding line, as part of the overburden pressure is supported by basal water or sea water and basal motion therefore facilitated.

25 At the same time the method, as applied here, does not lead to a full reproduction of the surface flow structure. This suggests that other processes, not considered here, are also important for the basal sliding behaviour. A possibility not tested yet due to time constraints is the effect of the basal stress exponent  $p$ . Increasing it would to some extent perhaps regulate the high velocities in some areas, due to low basal stresses.

5 The locations of the fast flowing tributaries and the central stream are well indicated by a temperate base. The structure is visible even more clearly than for the reference simulation. This supports the idea that the location of some tributaries is influenced by basal temperatures.

10 For the second new parametrisation for basal sliding we test the applicability of a theory developed by Li et al. (2010) to the region of PIG, that connects a ~~two-parameter roughness index~~ two-parameter roughness measure  $\{\xi_2, \eta_2\}$  to the basal sliding law. We rewrite the equations from Li et al. (2010), by partly using information of the original ideas from Weertman (1957), and extend the sliding law with a temperature function  $f(T)$ , to apply it as a boundary condition in our flow model. We define a constant sliding parameter  $C_L$ , over which a parameter study is conducted.

15 The results of the surface flow field show certain features. The central stream in all the simulations from this section is partitioned into a faster flowing upper part, and a slower flowing lower part, in the vicinity of the ice shelf. No single value for  $C_L$  could be found, that reproduces the surface velocity field of PIG with all its features. For higher  $C_L$  values, that reproduce the velocities in the central stream in a better manner, the velocities in the slower flowing area around tributaries 3, 5, 7 and 9, located to the South of the main stream, are simulated much too high (cf. Fig. 11c)). Additionally, the area around tributary 14 behaves slightly different to most other tributaries. It flows much faster for much lower values of  $C_L$ .  
20 This is related to the low roughness measures  $\xi_2$  and  $\eta_2$  in that region.

Thus, despite the inability of a complete reproduction of the surface flow field of PIG with the method presented here, it still resulted in a surface flow structure, that reveals some important features, like the location of the fast flowing central stream and some of the numerous tributaries.

## 6 Conclusions

The overall motion of the fast flowing parts of PIG are dominated by basal motion. The parametrisation of basal motion is therefore crucial for simulating the flow of PIG. Especially when running prognostic simulations of the glacier and aiming at analysing the stability of the system, parametrisation of basal motion is important. High subglacial erosion rates are likely to change the subglacial environment over time. Also the basal temperature plays an important role in separating fast sliding regions from regions dominated by internal deformation. We introduced two different approaches of connecting a basal sliding formulation to an actually measurable subglacial parameter, the basal roughness measure. Our results show, that the roughness measure is a very useful parameter to be considered for parametrisation of basal motion at PIG, as important features of the flow field could be reproduced. Nonetheless the full complexity of the problem was not captured. Our approach is a step towards a more physically based parametrisation for basal sliding, which is very important for realistic simulations of glacier dynamics.

*Acknowledgements.* This work was supported through the Cluster of Excellence 'CliSAP' (EXC177), University of Hamburg, funded through the German Science Foundation (DFG). We would like to thank Anne Le Brocq for providing the compiled data set for the geometry of Pine Island Glacier.

## References

Bamber, J., Gomez-Dans, J., , and Griggs, J.: A new 1km digital elevation model of the Antarctic derived from combined satellite radar and laser data – Part 1: Data and methods, THE CRYOSPHERE, 3, 101–111, doi:10.5194/tc-3-101-2009, 2009.

- Bindschadler, R.: The importance of pressurized subglacial water in separation and sliding at the glacier bed, *J GLACIOL*, 29, 3–19, 1983.
- 25 Bingham, R. and Siegert, M.: Quantifying subglacial bed roughness in Antarctica: implications for ice-sheet dynamics and history, *QUATERNARY SCI REV*, 28, 223–236, 2009.
- Blatter, H. and Hutter, K.: Polythermal conditions in Arctic glaciers, *J GLACIOL*, 37, 261–269, 1991.
- Bohlander, J. and Scambos, T.: Antarctic coastlines and grounding line derived from MODIS Mosaic of Antarctica (MOA), National Snow and Ice Data Center, Digital media, accessed 24 April 2008., Boulder, Colorado USA, 2007.
- 30 Budd, W. and Jenssen, D.: Numerical modelling of the large-scale basal water flux under the West Antarctic Ice Sheet, in: *Dynamics of the West Antarctic Ice Sheet*, edited by Van der Veen, C. J. and Oerlemans, J., p. 293–320, Kluwer, Dordrecht, 1987.
- Codina, R.: Comparison of some finite element methods for solving the diffusion-convection-reaction equation, *COMPUT METHOD APPL M*, 156, 185–210, doi:10.1016/S0045-7825(97)00206-5, 1998.
- Comiso, J.: Variability and Trends in Antarctic surface temperatures from in situ and satellite infrared measurements, *J CLIMATE*, 13, 1674–1696, 2000.
- 5 COMSOL: COMSOL Multiphysics Reference Guide, COMSOL AB, Vers. 4.3a, [http://www.comsol.com/\(lastaccess:10August2014\)](http://www.comsol.com/(lastaccess:10August2014)), 2012.
- Cornford, S., Martin, D., Graves, D., Ranken, D., Le Brocq, A., Gladstone, R., Payne, A., Ng, E., and Lipscomb, W.: Adaptive mesh, finite volume modeling of marine ice sheets, *J COMPUT PHYS*, 232, 529–549, 2012.
- 10 Cuffey, K. M. and Paterson, W. S. B.: *The Physics of Glaciers*, Butterworth-Heinemann, 4th edn., 2010.
- Dutrieux, P., De Rydt, J., Jenkins, A., Holland, P., Ha, H., Lee, S., Steig, E., Ding, Q., Abrahamsen, E., and Schröder, M.: Strong sensitivity of Pine Island ice-shelf melting to climatic variability, *SCIENCE*, 343, 174–178, 2014.
- 15 Favier, L., Durand, G., Cornford, S., Gudmundsson, G., Gagliardini, O., Gillet-Chaulet, F., Zwinger, T., Payne, A., and Le Brocq, A.: Retreat of Pine Island Glacier controlled by marine ice-sheet instability, *NATURE CLIMATE CHANGE*, 4, 117–121, doi:10.1038/NCLIMATE2094, 2014.
- Fowler, A.: A sliding law for glaciers of constant viscosity in the presence of subglacial cavitation, *P R SOC A*, 407, 147–170, 1986.
- 20 Fox Maule, C., Purucker, M., Olsen, N., and Mosegaard, K.: Heat flux anomalies in Antarctica revealed by satellite magnetic data, *SCIENCE*, 309, 464–467, 2005.

- 25 Gladstone, R., Lee, V., Rougier, J., Payne, A., Hellmer, H., Brocq, A. L., Shepherd, A., Edwards, T., Gregory, J., and Cornford, S.: Calibrated prediction of Pine Island Glacier retreat during the 21st and 22nd centuries with a coupled flowline model, *EARTH PLANET SC LETT*, 333-334, 191–199, 2012.
- Glen, J.: The creep of polycrystalline ice, *P R SOC A*, 228, 519–538, 1955.
- Greve, R. and Blatter, H.: *Dynamics of Ice Sheets and Glaciers*, Springer, Berlin, Heidelberg, 2009.
- 30 Gudmundsson, G., Krug, J., Durand, G., Favier, L., and Gagliardini, O.: The stability of grounding lines on retrograde slopes, *THE CRYOSPHERE*, 6, 1497–1505, doi:10.5194/tc-6-1497-2012, 2012.
- Hauke, G. and Hughes, T. J.: A comparative study of different sets of variables for solving compressible and incompressible flows, *COMPUT METHOD APPL M*, 153, 1–44, doi:10.1016/S0045-7825(97)00043-1, 1998.
- Hooke, R. L.: *Principles of Glacier Mechanics*, Cambridge University Press, Cambridge, 2005.
- Horwath, M. and Dietrich, R.: Signal and error in mass change inferences from GRACE: the case of Antarctica, *GEOPHYS J INT*, 177, 849–864, 2009.
- 5 Hubbard, B., Siegert, M., and McCarroll, D.: Spectral roughness of glaciated bedrock geomorphic surfaces: implications for glacier sliding, *J GEOPHYS RES*, 105, 21 295–21 303, 2000.
- Hughes, T.: Is the West Antarctic ice sheet disintegrating?, *J GEOPHYS RES*, 78, 7884–7910, 1973.
- Humbert, A., Kleiner, T., Mohrholz, C., Oelke, C., Greve, R., and Lange, M.: A comparative modeling study of the Brunt Ice Shelf/Stancomb-Wills Ice Tongue system, East Antarctica, *J GLACIOL*, 55, 53–65, 2009.
- 10 Hutter, K.: *Theoretical glaciology: Material Science of Ice and the Mechanics of Glaciers and Ice Sheets*, Reidel, Tokyo, 1983.
- Huybrechts, P.: The Antarctic ice sheet and environmental change: a three-dimensional modelling study, *REPORTS ON POLAR RESEARCH*, Alfred Wegener Institute for Polar and Marine Research, Bremerhaven, 99, 1992.
- 15 Joughin, I., Tulaczyk, S., Bamber, J., Blankenship, D., Holt, J., Scambos, T., and Vaughan, D.: Basal conditions for Pine Island and Thwaites Glaciers, West Antarctica, determined using satellite and airborne data, *J GLACIOL*, 55, 245–257, 2009.
- Joughin, I., Smith, B., and Holland, D.: Sensitivity of 21st century sea level to ocean-induced thinning of Pine Island Glacier, Antarctica, *GEOPHYS RES LETT*, 37, L20 502, doi:10.1029/2010GL044819, 2010.
- 20

- Kamb, B.: Sliding motion of glaciers: theory and observations, *Reviews of Geophysics and Space Physics*, 8, 673–728, 1970.
- Karlsson, N., Rippin, D., Vaughan, D., and Corr, H.: The internal layering of Pine Island Glacier, West Antarctica, from airborne radar-sounding data, *ANN GLACIOL*, 50, 141–146, 2009.
- Katz, R. and Worster, M.: Stability of ice-sheet grounding lines, *P R SOC A*, 466, 1597–1620, 2010.
- Kleiner, T. and Humbert, A.: Numerical simulations of major ice streams in western Dronning Maud Land, Antarctica, under wet and dry basal conditions, *J GLACIOL*, 60, 215–232, 2014.
- Le Brocq, A., Payne, A., and Vieli, A.: An improved Antarctic dataset for high resolution numerical ice sheet models (ALBMAP v1), *EARTH SYST SCI DATA*, 2, 247–260, doi:10.5194/essd-2-247-2010, 2010.
- Leguy, G. R., Asay-Davis, X. S., and Lipscomb, W. H.: Parameterization of basal friction near grounding lines in a one-dimensional ice sheet model, *THE CRYOSPHERE*, 8, 1239–1259, doi:10.5194/tc-8-1239-2014, 2014.
- Li, X., Sun, B., Siegert, M., Bingham, R., Tang, X., Zhang, D., Cui, X., and Zhang, X.: Characterization of subglacial landscapes by a two-parameter roughness index, *J GLACIOL*, 56, 831–836, 2010.
- MacAyeal, D.: The basal stress distribution of Ice Stream E, Antarctica, inferred by control methods, *J GEOPHYS RES*, 97, 595–603, 1992.
- Morland, L.: Thermomechanical balances of ice sheet flows, *GEOPHYS ASTRO FLUID*, 29, 237–266, 1984.
- Morlighem, M., Rignot, E., Seroussi, H., Larour, E., Ben Dhia, H., and Aubry, D.: Spatial patterns of basal drag inferred using control methods from a full-Stokes and simpler models for Pine Island Glacier, West Antarctica, *GEOPHYS RES LETT*, 37, L14 502, doi:10.1029/2010GL043853, 2010.
- Mouginot, J., Rignot, E., and Scheuchl, B.: Sustained increase in ice discharge from the Amundsen Sea Embayment, West Antarctica, from 1973 to 2013, *GEOPHYS RES LETT*, 41, 1576–1584, doi:10.1002/2013GL059069, 2014.
- Nye, J.: The distribution of stress and velocity in glaciers and ice-sheets, *P R SOC A*, 239, 113–133, 1957.
- Nye, J.: The calculation of sliding of ice over a wavy surface using Newtonian viscous approximation, *P R SOC A*, A311, 445–467, 1969.
- Park, J., Gourmelen, N., Shepherd, A., Kim, S., Vaughan, D., and Wingham, D.: Sustained retreat of the Pine Island Glacier, *GEOPHYS RES LETT*, 40, 1–6, 2013.
- Paterson, W.: *The Physics of Glaciers*, Elsevier, Oxford, 1994.

- Pattyn, F.: A new three-dimensional higher-order thermomechanical ice sheet model: basic sensitivity, ice stream development, and ice flow across subglacial lakes, *J GEOPHYS RES*, 108, 2382, doi:10.1029/2002JB002329, 2003.
- 25 Pattyn, F., Perichon, L., Durand, G., Favier, L., Gagliardini, O., Hindmarsh, R. C., Zwinger, T., Albrecht, T., Cornford, S., Docquier, D., Fürst, J., Goldberg, D., Gudmundsson, H., Humbert, A., Hutten, M., Huybrechts, P., Jouvét, G., Kleiner, T., Larour, E., Martin, D., Morlighem, M., Payne, A., Pollard, D., Rückamp, M., Rybak, O., Seroussi, H., Thoma, M., and Wilkens, N.: Grounding-line migration in plan-view marine ice-sheet models: results of the ice2sea MISMIP3d intercomparison, *J GLACIOL*, 59, 2163, doi:10.3189/2013JoG12J129, 2013.
- 30 Rignot, E.: Fast recession of a West Antarctic glacier, *SCIENCE*, 281, 549–551, 1998.
- Rignot, E.: Ice-shelf changes in Pine Island Bay, Antarctica, 1947-2000, *J GLACIOL*, 48, 247–256, 2002.
- Rignot, E.: Changes in West Antarctic ice stream dynamics observed with ALOS PALSAR data, *GEOPHYS RES LETT*, 35, L12 505, doi:10.1029/2008GL033365, 2008.
- Rignot, E., Mouginot, J., and Scheuchl, B.: Ice flow of the Antarctic ice sheet, *SCIENCE*, 333, 1427–  
5 1430, 2011.
- Rippin, D., Vaughan, D., and Corr, H.: The basal roughness of Pine Island Glacier, West Antarctica, *J GLACIOL*, 57, 67–76, 2011.
- Rippin, D., Bingham, R., Jordan, T., Wright, A., Ross, N., Corr, H., Ferraccioli, F., Le Brocq, A., Rose, K., and Siegert, M.: Basal roughness of the Institute and Möller Ice Streams, West Antarctica: process determination and landscape interpretation, *GEOMORPHOLOGY*, 214, 139–147, 2014.
- 10 Rückamp, M.: Eisgeometrie und Fließdynamik der subpolaren Eiskappe von King George Island (Antarktis), Ph.D. thesis, Universität Münster, Münster, 2011.
- Schmeltz, M., Rignot, E., Dupont, T., and MacAyeal, D.: Sensitivity of Pine Island Glacier, West Antarctica, to changes in ice-shelf and basal conditions: a model study, *J GLACIOL*, 48, 552–  
15 558, 2002.
- Seroussi, H., Morlighem, M., Rignot, E., Mouginot, J., Larour, E., Schodlok, M., and Khazendar, A.: Sensitivity of the dynamics of Pine Island Glacier, West Antarctica, to climate forcing for the next 50 years, *THE CRYOSPHERE DISCUSS*, 8, 1873–1894, doi:10.5194/tcd-8-1873-2014, 2014.
- 20 Shepherd, A., Ivins, E. R., A, G., Barletta, V. R., Bentley, M. J., Bettadpur, S., Briggs, K. H., Bromwich, D. H., Forsberg, R., Galin, N., Horwath, M., Jacobs, S., Joughin, I., King, M. A., Lenaerts, J. T. M., Li, J., Ligtenberg, S. R. M., Luckman, A., Luthcke, S. B., McMillan, M., Meister, R., Milne, G., Mouginot, J., Muir, A., Nicolas, J. P., Paden, J., Payne, A. J., Pritchard, H., Rignot, E., Rott, H.,



- 25 Sandberg Sørensen, L., Scambos, T. A., Scheuchl, B., Schrama, E. J. O., Smith, B., Sundal, A. V., van Angelen, J. H., van de Berg, W. J., van den Broeke, M. R., Vaughan, D. G., Velicogna, I., Wahr, J., Whitehouse, P. L., Wingham, D. J., Yi, D., Young, D., and Zwally, H. J.: A reconciled estimate of ice-sheet mass balance, *SCIENCE*, 338, 1183–1189, 2012.
- Smith, A., Bentley, C., Bingham, R., and Jordan, T.: Rapid subglacial erosion beneath Pine Island Glacier, West Antarctica, *GEOPHYS RES LETT*, 39, L12 501, doi:10.1029/2012GL051651, 2012.
- Smith, A., Jordan, T., Ferraccioli, F., and Bingham, R.: Influence of subglacial conditions on ice stream dynamics: Seismic and potential field data from Pine Island Glacier, West Antarctica, *J*  
925 *GEOPHYS RES*, 118, 1471–1482, 2013.
- Stenoien, M. and Bentley, C.: Pine Island Glacier, Antarctica: A study of the catchment using interferometric synthetic aperture radar measurements and radar altimetry, *J GEOPHYS RES*, 105, 21 761–21 779, 2000.
- Taylor, J., Siegert, M. J., Payne, A. J., and Hubbard, B.: Regional-scale bed roughness beneath ice masses: measurement and analysis, *COMPUT GEOSCI*, 30, 899–908, 2004.
- 930 Vaughan, D.: West Antarctic Ice Sheet collapse - the fall and rise of a paradigm, *CLIMATIC CHANGE*, 91, 65–79, 2008.
- Vaughan, D., Corr, H., Ferraccioli, F., Frearson, N., O'Hare, A., Mach, D., Holt, J., Blankenship, D., Morse, D., and Young, D.: New boundary conditions for the West Antarctic ice sheet: subglacial topography beneath Pine Island Glacier, *GEOPHYS RES LETT*, 33, L09 501, doi:10.1029/2005GL025588, 2006.
- Vaughan, D., Corr, H., Bindschadler, R., Dutrieux, P., Gudmundsson, G., Jenkins, A., Newman, T., Vornberger, P., and Wingham, D.: Subglacial melt channels and fracture in the floating part of Pine Island Glacier, Antarctica, *J GEOPHYS RES*, 117, F03 012, doi:10.1029/2012JF002360, 2012.
- 940 Weertman, J.: On the sliding of glaciers, *J GLACIOL*, 3, 33–38, 1957.
- Weis, M., Greve, R., and Hutter, K.: Theory of shallow ice shelves, *CONTINUUM MECH THERM*, 11, 15–50, 1999.
- Wilkens, N.: Pine Island Glacier - a 3D full-Stokes model study, Ph.D. thesis, Universität Hamburg, Hamburg, <http://ediss.sub.uni-hamburg.de/volltexte/2014/6735/>, [http://ediss.sub.uni-hamburg.de/volltexte/2014/6735/\(lastaccess:18August2014\)](http://ediss.sub.uni-hamburg.de/volltexte/2014/6735/(lastaccess:18August2014)), 2014.
- 945 Wingham, D., Wallis, D., and Shepherd, A.: Spatial and temporal evolution of Pine Island Glacier thinning, 1995–2006, *GEOPHYS RES LETT*, 36, L17 501, doi:10.1029/2009GL039126, 2009.

**Table 1.** Parameter Values

Parameter	Value	Unit	Description
$\rho_i$	918	$\text{kg m}^{-3}$	Ice density
$\rho_w$ <i><math>\rho_{sw}</math></i>	1028	$\text{kg m}^{-3}$	Seawater density
$g$	9.81	$\text{m s}^{-2}$	Acceleration of gravity
$n$	3		Stress exponent
$R$	8.314	$\text{J mol}^{-1} \text{K}^{-1}$	Gas constant
$Q$	60 for $T' \leq 263.15 \text{ K}$ 139 for $T' > 263.15 \text{ K}$	$\text{kJ mol}^{-1}$	Activation energy for creep ( <a href="#">Paterson, 1994</a> )
$A_0$	$3.985 \times 10^{-13}$ for $T' \leq 263.15 \text{ K}$ $1.916 \times 10^3$ for $T' > 263.15 \text{ K}$	$\text{s}^{-1} \text{Pa}^{-3}$	Pre-exponential constant ( <a href="#">Paterson, 1994</a> )
$T_0$	273.15	K	Melting point for low pressures
$\beta_c$	$9.8 \times 10^{-8}$	$\text{K Pa}^{-1}$	Clausius-Clapeyron constant (Hooke, 2005)
$T_{sw}$	271.15	K	Freezing temperature of seawater
$\nu$	0.1		Submelt sliding parameter (Budd and Jenssen, 1987)
$\kappa(T)$	$9.828 e^{(-5.7 \times 10^{-3} T [\text{K}^{-1}])}$	$\text{W m}^{-1} \text{K}^{-1}$	Thermal conductivity
$c_p(T)$	$152.5 + 7.122 T [\text{K}^{-1}]$	$\text{J kg}^{-1} \text{K}^{-1}$	Specific heat capacity
$z_{sl}$	0	m	Sea level
$spy$	31536000	$\text{s a}^{-1}$	Seconds per year

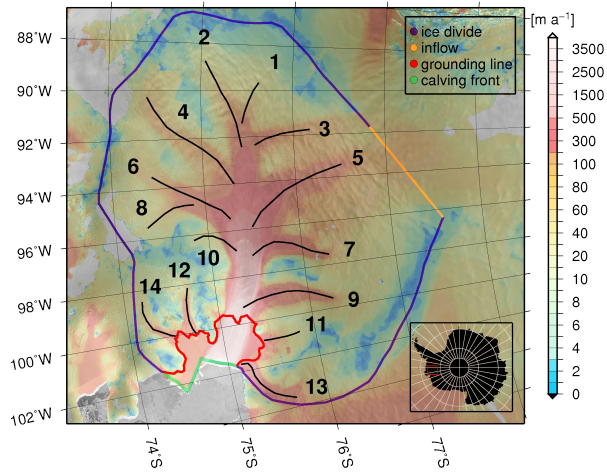


**Figure 1.** RADARSAT Antarctic Mapping Project (RAMP) Mosaic with the observed surface velocities from Rignot et al. (2011) and the model domain of Pine Island Glacier, with the different lateral boundaries, the grounding line and the numbered tributaries indicated.

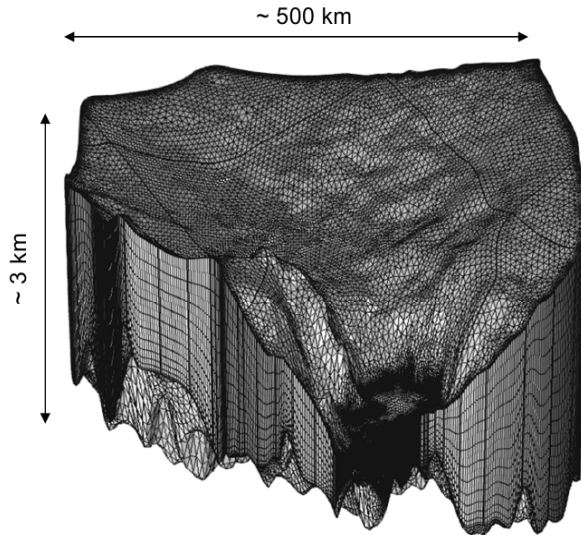


**Figure 2.** FEM mesh on the 3D Pine Island Glacier model geometry.

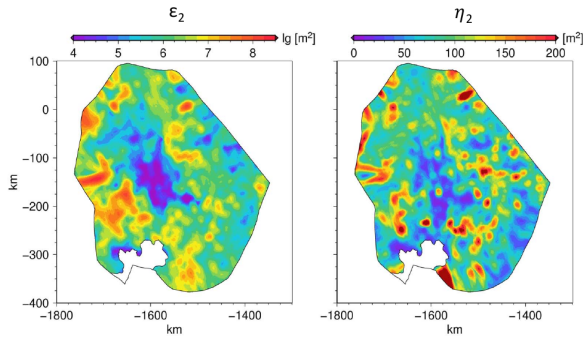


**Figure 3.** The two-parameter roughness measure at Pine Island Glacier, given by the roughness amplitude  $\xi_2$  and the roughness frequency  $\eta_2$ .

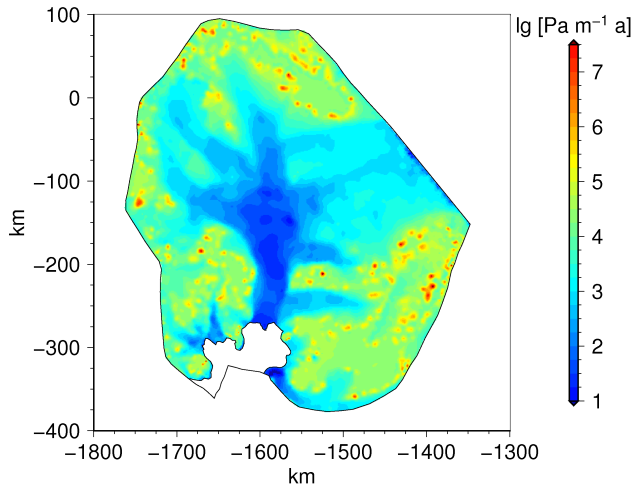


**Figure 4.** Spatial distribution of the basal sliding parameter  $\beta^2$ .

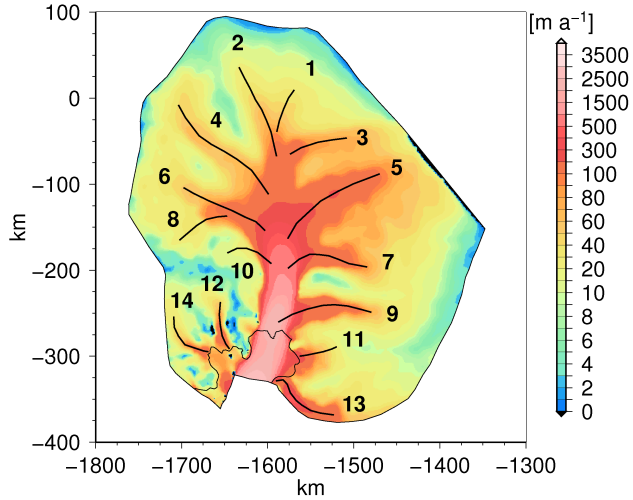


**Figure 5.** Surface velocity field from the reference simulation  $|u_{s,\text{ref}}|$ , with the numbered tributaries.

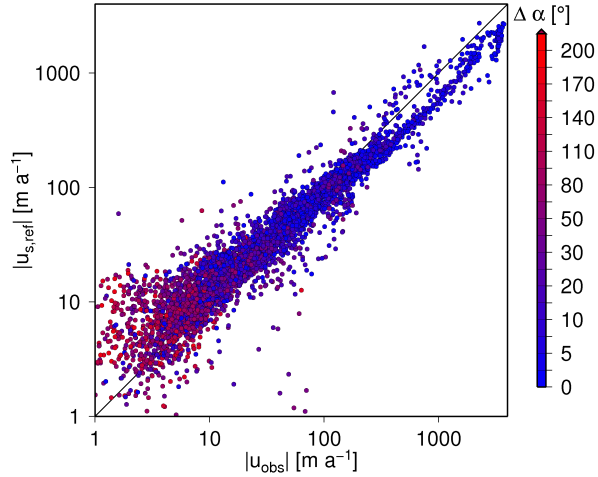


**Figure 6.** Observed surface velocity field  $|u_{\text{obs}}|$  versus vs. reference surface velocity field  $|u_{\text{s,ref}}|$ ; with. The logarithmic scales exaggerate the spread around the low speeds. The angle offset  $\Delta\alpha$  between the vectors of the surface velocity field  $u_{\text{obs}}$  and the reference surface velocity field  $u_{\text{s,ref}}$  is shown as the colour code.



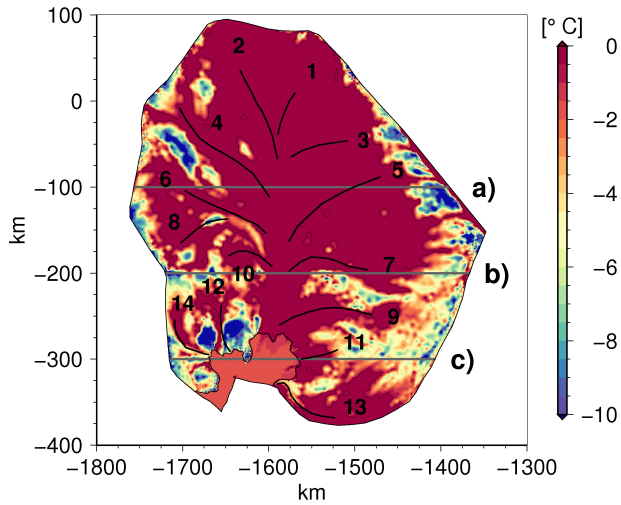


**Figure 7.** The basal homologous temperature from the reference simulation  $T'_{D,ref}$ , with tributary locations in black and the location of the vertical slices a), b) and c) in Fig. 8 in grey.

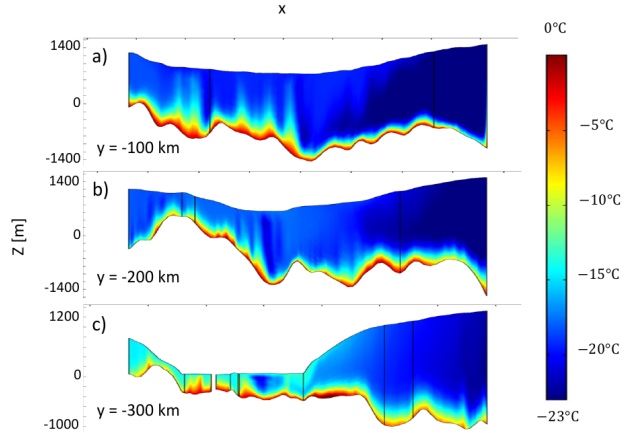


**Figure 8.** The internal homologous temperature from the reference simulation  $T'_{\text{ref}}$  at three vertical slices a), b) and c) (horizontal locations indicated in Fig. 7)

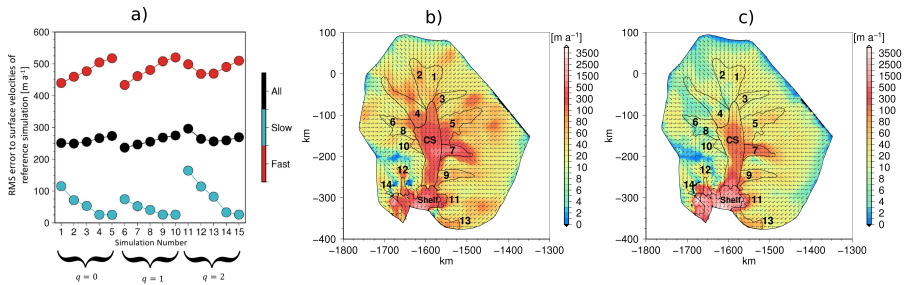


**Figure 9.** a) RMS error to the surface velocity field of the reference simulation versus the simulation number; b) Surface velocity field of simulation 2 with  $q = 0$ ; c) Surface velocity field of simulation 11 with  $q = 2$ .

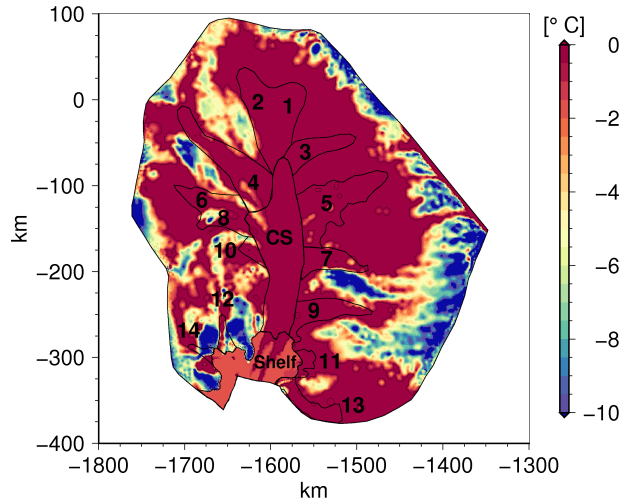


**Figure 10.** Basal homologous temperature of simulation 2  $T'_{b,p1q0\_2}$ .

The two parameter roughness measure at Pine Island Glacier, given by the roughness amplitude  $\xi_2$  and the roughness frequency  $\eta_2$ .

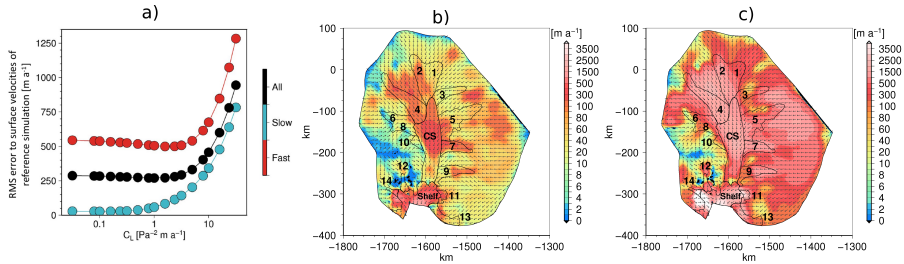


**Figure 11.** a) RMS error to the surface velocity field of the reference simulation versus  $C_L$  value; b) Surface velocity field with  $C_L = 1 \text{ Pa}^{-2} \text{m a}^{-1}$ ; c) Surface velocity field with  $C_L = 31.56 \text{ Pa}^{-2} \text{m a}^{-1}$ .